THE STRUCTURE OF THE LARGE MAGELLANIC CLOUD

By

Oyirwoth Patrick Abedigamba

A dissertation submitted in partial fulfillment of the requirements for the degree M.Sc. in the Department of Astronomy, as part of the National Astrophysics and Space Science Programme

UNIVERSITY OF CAPE TOWN

AUGUST 2010

Supervisors:

Honorary. Prof. Michael Feast[1,2]

Prof. Patricia Whitelock[2,1]

[1]Astronomy Department, University of Cape Town

[2]South African Astronomical Observatory

Key words

Large Magellanic Cloud, RR Lyrae stars, Optical Gravitational Lensing Experiment, Fourier parameters, metallicity [Fe/H].

Abstract

This work gives an account of the study of the metallicity [Fe/H] distribution (gradient) in the oldest population in the Large Magellanic Cloud (LMC), by making use of the available RR Lyrae data from the Optical Gravitational Lensing Experiment III (OGLE III). RR Lyrae stars are amongst the oldest objects in the universe and they have a range in element (metal) abundances. Measuring the distribution of metallicities of RR Lyrae stars in a galaxy gives one clues to the origin of galaxies. It is known that the pulsation periods of RR Lyraes is broadly correlated with their metallicity. This fact has been used for investigating the metallicity distribution of RR Lyrae stars in the LMC. I have found an indication that the proportion of metal poor RR Lyrae stars increases with distance from the centre of the LMC. In addition, an attempt was made to improve the metallicity-period relation by introducing the Fourier parameters, but this was unsuccessful. Lastly, a comparison is made with estimates of metallicity gradients of other LMC populations.

Declaration

I declare that *The structure of the Large Magellanic Cloud* is my own work and with the advice of my supervisors, that it has not been submitted for any degree or examination in any other university, and that all the sources I have used or quoted have been indicated and acknowledged by complete references.

Copyright and Intellectual property right

Oyirwoth Patrick Abedigamba

Acknowledgments

I wish to thank the National Astrophysics and Space Science Program (NASSP) for giving me an opportunity to gain knowledge in this field of study. I wish to thank my supervisors Prof. Micheal Feast and Prof. Patricia Whitelock for patiently guiding and supporting me throughout this work. In addition, I would like to extend my sincere thanks to Dr. Maria-Rosa L. Cioni (University of Hertfordshire) for the wonderful internet discussions given to me pertaining this work whenever I needed some assistance, Dr. A Layden for providing us with his private communication data, and not forgetting Dr. Bruno Lertate in our research group at the South African Astronomical Observatory (S.A.A.O) for the wonderful contributions towards this project. In a special way I would like to say many thanks to the librarians Davis Shireen and Ntsham Nomgcobo of S.A.A.O.

I also extend my gratitude and appreciation to the University of Cape Town (UCT) and the South African Astronomical Observatory (SAAO) for all the moral and financial support. In a special way I would like to appreciate the help offered by the Information Technology (IT) departments of UCT, SAAO and NASSP who have been there for me whenever I was in trouble with my computer.

I would like also to thank Dr. Edward Jurua for his educational & moral support and all my friends for all the help rendered most especially Zara.

I also extend my appreciation to my family members who have been there for me in terms of encouragement and support for all this period when I was away from them.

Above all, I thank the Almighty God for guiding and protecting me during this duration of time. Let his name be Glorified!!.

This dissertation makes use of data from the Optical Gravitational Lensing Experiment

III (OGLE III), which is a joint project of Warsaw University, Princeton University and the Carnegie institution, and is a Polish Astronomical project at Las Campanas Observatory Chile.

Contents

Chapter 1

Introduction

The aim of this study is an in-depth investigation of the structure of the Large Magellanic Cloud (LMC). The LMC is a nearby satellite galaxy that is interacting gravitationally with our Milky Way. Given its close proximity, the LMC offers us a unique opportunity to study in detail the dynamics and composition of another galaxy.
An interesting theme in all Magellanic Cloud research is their evolution and present structure. Important topics like chemical composition, evolution and kinematics are the current research interests in the area of the Magellanic Clouds. This dissertation focusses on the investigation of a possible metallicity gradient in the LMC.

1.1 Problem statement

RR Lyrae stars are representative of the oldest populations of stars in the universe. Because they are easily recognised in our own and other galaxies, they are crucial objects for studies of these old populations. The abundance of the chemical elements ("metallicity") varies in different samples of RR Lyrae variables. Various authors (e.g. Sandage, 1993; Layden, 1995; Sarajedini et al., 2006) have recently predicted that the metallicity of RR Lyrae stars depends on period while others suggested that metallicity depends on period and Fourier parameters (e.g. Jurcsik & Kovács, 1996; Alcock et al., 2000). It is one of the aims of this project to test these suggestions and investigate the metallicity distribution in the LMC using the RR Lyrae stars from the Optical

Gravitational Lensing Experiment III (Soszyński et al., 2009)(=OGLE III).

1.2 Specific aim and objective of the study

(i) To derive metallicity, period and Fourier parameter (phase or amplitude) relations for RR Lyrae stars in the LMC.
(ii) To study the metallicity distribution in the oldest population in the LMC, i.e. to see whether there is a metallicity gradient or not in the LMC, by making use of the RR Lyrae stars from OGLE III.

1.3 Outline of the dissertation

The dissertation consists of five chapters.

Chapter one is a literature review of the known information on the Magellanic Clouds with emphasis on the Large Magellanic Cloud and RR Lyrae stars.

Chapter two is a discussion of the derivation of iron abundances from the period and light curve shapes of RR Lyrae stars. OGLE III is discussed here as well as the data and method used in the analysis.

Chapter three is a discussion of the metallicity as a function of galactocentric distance as derived from the periods of RR Lyrae stars in the LMC with some information on the Weighted Least Square Straight Line Fitting. A comparison is made with the metallicity gradients of other LMC populations e.g. Asymptotic Giant Branch (AGB) stars, stellar clusters and HII regions.

Chapter four discusses an alternative way to study the LMC metallicity gradient of RR Lyrae variables by using selection criteria according to space density for samples with and without the bright stars.

Chapter five is the general conclusion & recommendation and the way forward (future work) .

Finally, the χ^2 test used in analysing the data and the interpretation of the χ^2 values in connection to this work is presented in an Appendix.

1.4 The Magellanic Clouds

The Magellanic Clouds have been known for thousands of years to the inhabitants of the Southern hemisphere. The Australian aborigines considered the Magellanic Cloud as two black men who sometimes came down to the Earth and choked people while they were asleep (McCarthy, 1956).

The two objects were called the Cape Clouds for hundreds of years; they were the most striking objects appearing in the sky when ships approached the Cape of Good Hope, where there is no star corresponding to Polaris in the North (Allen, 1980). The Clouds became connected with the name of the Portuguese seafarer Magalhaes through Antonio Pigafetta's narrative of the first circumnavigation of the globe.

Pigafetta (1524) documented that: 'The Antarctic Pole is not so marked by stars as the Arctic. For you see there are several small stars clustered together, in the manner of two clouds a little seperated from one another, and somewhat dim. Now in the middle of them are two stars not very large, not very bright, and they move slightly. And these two stars are the Antarctic pole'. As a result of this valuable narrative, the Clouds were later named Magellanic Clouds, i.e. the Large Magellanic Cloud (LMC) and the Small Magellanic Cloud (SMC).

The unique character of the Magellanic Clouds has been recognised since the days of John Herschel, who gave their coordinates and the description of 244 objects in the SMC and 919 in the LMC.

It is now well known that the Magellanic Clouds are two nearby companions of the Milky Way (i.e. satellites to our own Galaxy). To the naked eye, the two Magellanic

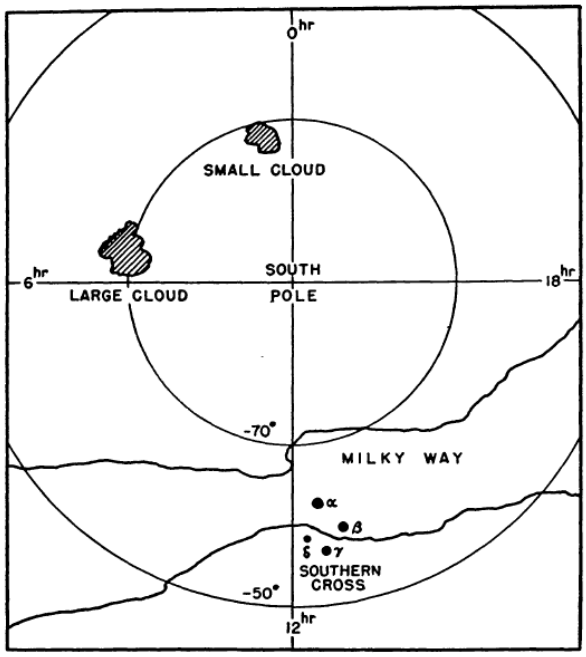

Figure 1.1: Region of the South Pole, showing the relative positions of the Magellanic Clouds, the Southern Cross, and the Milky Way, adopted from Buscombe (1954).

Clouds look like detatched portion of the Milky way, well out of the Galactic plane at Galactic latitudes 30° and 48° respectively. When viewed from outside our Galaxy, the Clouds would appear to be satellites situated 5 to 6 times as far from the Galactic nucleus as the sun and with diameters rather less than half that distance (Alcaino, 1975). Therefore, because they are close companion galaxies to our own and at well known distances, they offer us opportunity to study individual stars.

Due to their importance, many survey projects have been carried out which monitored the sky toward the Magellanic Clouds, one of the most complete variable stars surveys being the OGLE III survey.

1.4.1 The Large Magellanic Cloud

The Large Magellanic Cloud (LMC) is known to be an Irregular galaxy (Irr I) according to the Hubble scheme (Sandage, 1961; Binney & Merrifield, 1998 page 148; Carroll & Ostlie, 1996). It is an important probe of galaxy formation history. Many authors (e.g. Van der Marel et al., 2002, Nikolaev et al., 2006) have carried out studies on the struc-

ture and evolution of the Large Magellanic Cloud. The LMC contains different kinds of variable stars, e.g. Classical Cepheids (Soszyński et al., 2008a), Type II Cepheids (Soszyński et al., 2008b), RR Lyrae (Soszyński et al., 2009), δ scuti stars (Poleski et al., 2010).

Feast (1968) found out that for the LMC, the velocity dispersion of the planetaries corrected for observational errors is 22±3 kms^{-1} greater than that of extreme population - I objects, which is 9.6±1.1 kms^{-1} showing that the OB stars are in the disc while the planetary Nebulea are in the halo or thick disc.

The LMC contains a bar, covering an area in the sky of $\sim 3^{\circ} \times 1^{\circ}$, with its major axis in position angle (PA) 120° and its centre is at $5^h24^m.0$, -69°47′. The centre of the LMC has been defined as the position of the "radio centre of the rotation" and it was originally defined by the condition that the velocity curve resulting from the 21cm observations should be symmetrical so that the mass of the LMC could be derived.

Table 1.1 contains some of the known properties of the LMC.

Table 1.1: Table showing the properties of LMC, adopted from Westerlund (1997).

Properties	LMC
Galactic coord. l, b	280°.5,-32°.9
Distance modulus	18.5±0.2mag
RV_{hel}	275kms^{-1}
Integrated magnitude B	0.9 mag (100 deg^2)
Color B - V	0.5 mag
Central surface brightness	21.2 mag $arcsec^{-2}$
Total mass	$2\times10^{10}M\odot$

1.4.2 Magellanic Clouds as galaxies

Byrd et al. (1994) consider that the Magellanic Clouds may have left the M31 neighbourhood $\sim$ 10 Gyrs ago and may have been captured by our Galaxy $\sim$ 6 Gyrs ago. However, on the other side, Murai & Fujimoto (1980) examined the possibility that a single Magellanic Cloud was split into two independent objects, the LMC and the SMC, by tidal disruption at close passage to our Galaxy. Some of the known properties of the LMC can be seen in Table 1.2

Table 1.2: Some fundamental data for the LMC adopted from Westerlund (1997).

Structure:	**LMC**
Disk:	Has a major disk made up of intermediate age and young population (stars and gas)
Bar:	Red stars; superposed HII and stars forming regions

1.5 Populations in the LMC

1.5.1 The old, intermediate and young-age generations

In the LMC, the oldest generation of stars are those whose age $\geq$ 10 Gyrs, typical of old globular clusters.

The intermediate-generation have age $<$ 10 Gyrs and include objects like red giant stars, AGB stars including the carbon stars of which their numbers are estimated to be $\sim$ 12000 in the LMC (See Cioni, 2009; Cioni & Habing, 2003).

All the typical population I objects known in our Galaxy have been found in the LMC. The youngest population (age $\leq$ 100 Myrs) in the LMC are the OB stars, supergiants and hypergiants of type B-G (Feast et al., 1960).

1.5.2 The distance of the Large Magellanic Cloud

In an attempt to determine an accurate distance to the LMC in recent years, various types of variable stars have been used, e.g. Van Leeuwen et al. (2007) used Cepheids and found a distance modulus of 18.39$\pm$0.05, Clementini et al. (2003) used RR Lyrae stars and obtained a distance modulus of 18.50$\pm$0.07.

1.6 Stellar Pulsation

1.6.1 Driving pulsation (Kappa and Gamma Mechanisms)

The first physical mechanism behind pulsation was suggested in 1926 by Eddington (King & Cox, 1968; Eddington, 1929) who called it the 'valve' mechanism. The idea

was to see if a layer in the atmosphere releases heat during the compression stage or retains it. If the atmosphere retains it then the layer will contribute to the instability of the structure.

The opacity, kappa (κ) is the key factor which determines how radiation diffuses from the interior outwards. It depends on many parameters like the atoms involved, density, the wavelength of the radiation, but the most important one in understanding pulsation is the ionisation of matter. At some depth into the star there is a zone, above which hydrogen is neutral and below which it is completely ionized (partial ionization zone) while at some depth, there is a zone where helium is singly ionized and, deeper, a zone where it is doubly ionized. Outside the partial ionization zone, if a star is compressed, it heats up, the radiation flow increases and the opacity actually decreases which scales as $\kappa = \rho/T^{3.5}$ (Kramers Law). This therefore means that for a given shell, more energy is lost at the upper level than is received at the lower part. This radiative damping quickly damps out pulsation.

In the partial ionization zone, if a star is pulsating, as the star is compressed, the energy which would normally heat the zone mostly goes into increasing the ionization. This increases the opacity of the zone, trapping more radiation and resulting in outward pressure. This gives rise to damming of radiation (Gamma mechanism, γ). The zone is then driven outwards, cooling as it rises, which also increases the opacity and outward pressure. Further cooling of the zone gives rise in recombination of the ionized material and a sudden decrease in the opacity, a decrease in outward pressure and the zone drops back. If the zone is too deep in the star, it cannot drive against the overlying layers and if the zone is high, it has got nothing above it to drive. Location of the zone is critical in determining whether pulsation occurs and this explains why there are 'instability strips' in the HR diagram. The instability strips are areas where the stellar temperature is such that the driving zone is well located. For example, in stars like Classical Cepheids and RR Lyrae stars the driving zone is believed to be the second ionization of helium.

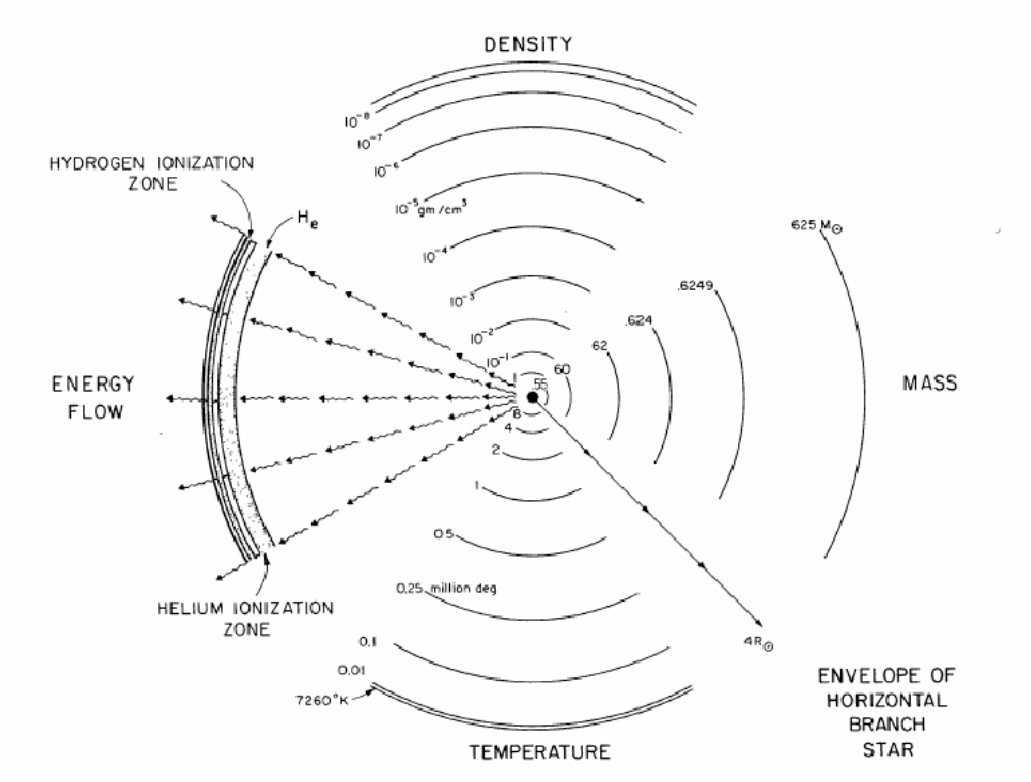

Figure 1.2: Distribution of the structure variables in the envelop of an initial horizontal branch model showing the helium and hydrogen ionisation zone. Adopted from Iben (1974).

1.6.2 Hertzsprung-Russell diagram (HR)

Stellar pulsations, either as radial with the star remaining spherical through the cycle or non-radial dynamical variabilities, where the shape deviates from the spherical, are found in many phases of stellar evolution and these variable stars occupy different regions on the HR diagram.

The dotted lines running almost vertically through Figure 1.3 approximate the location of the 'classical' instability strip. Going from high to low luminosities we find the Cepheids, RR Lyrae and δ scuti stars respectively. While other variables are situated at temperatures above the red edge of the instability strip at luminosities above $\sim 10^3 L_\odot$. These variables are indicated as, WR: Wolf - Rayet stars; LBV: Luminous blue variables.

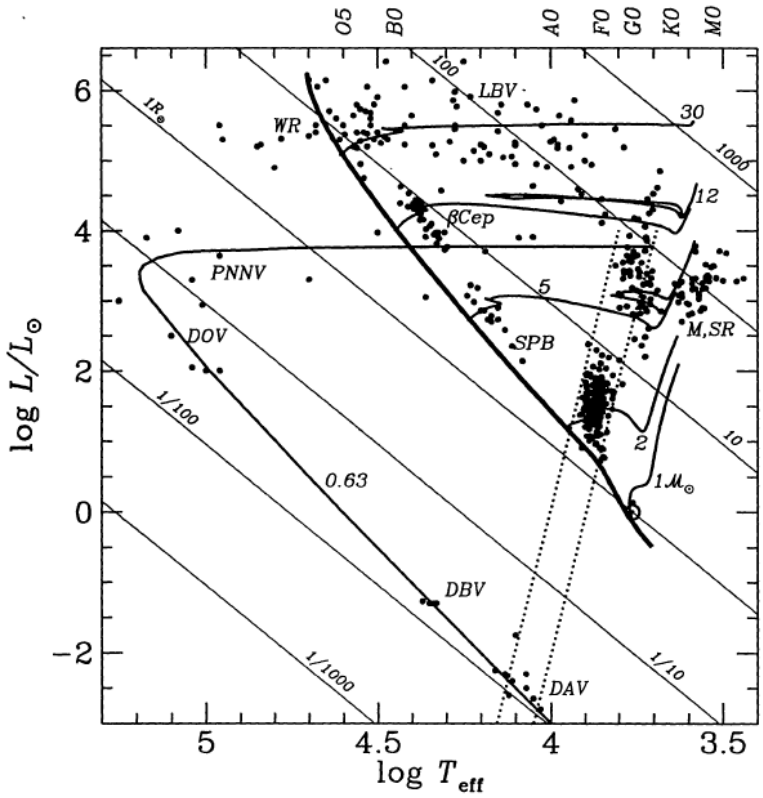

Figure 1.3: HR diagram showing the distribution of pulsating variables (dots), adopted from Gautschy & Saio (1995).

1.6.3 Pulsation periods

A non-varying star is relatively boring as an individual object; however, once a star pulsates, there is always a possibility to find out something about the interior of the star by matching observations with mathematical models of how stars should pulsate. In addition, pulsation sometimes gives us the ability to determine a parameter like metallicity, luminosity or distance.

The first calculations concerning stellar pulsation period was done by Ritter (1879) who showed that the period P of pulsation of a star is related to the density ρ by the equation $P\sqrt{\rho} = Q$, where Q is the pulsation constant.

1.7 RR Lyrae variables

The first RR Lyrae stars to be discovered in the Magellanic Clouds were in the SMC globular cluster NGC 121 and LMC globular cluster NGC 1466 (Thackeray & Wesselink, 1953). RR Lyrae stars are low-mass, radial pulsators, horizontal branch stars, typical of old stellar populations, periods of 0.2 - 1.1 days and light amplitudes from 0.2 mag to 2 mag in V (Kholopov et al., 1985). The onset of helium fusion puts the star on the horizontal branch at temperatures around 7000K ($\sim$ A type) and luminosities $\sim$ 50L$\odot$. RR Lyraes are moderately bright, easily recognised from their light variability, are distributed all over the LMC and have a range in metallicity values. Large numbers of RR Lyrae stars are found in the globular clusters and this explains why they are said to be old population stars.

The term "horizontal-branch" comes from the globular cluster color-magnitude (HR)

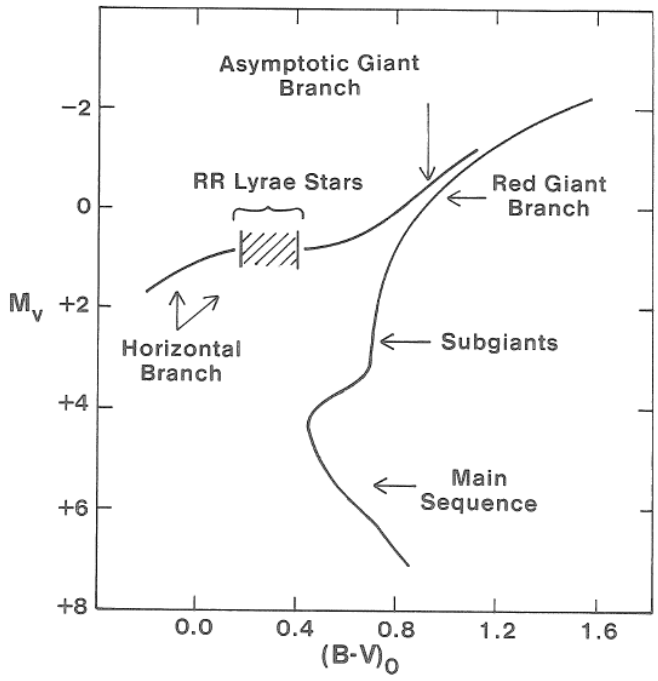

Figure 1.4: A schematic color-magnitude diagram for a typical Globular cluster showing the location of RR Lyrae stars. Adopted from Smith (1995).

diagram. Horizontal branch stars may be red (red horizontal branch stars - RHS), blue (Blue horizontal branch stars - BHB) or RR Lyrae variables. The ratio of RHB/BHB

stars is strongly variable and depends upon metallicity and age. It is important to point out that not all horizontal branch stars are RR Lyrae stars. It is only those within a well defined instability strip that are pulsationally unstable.

The following are some of the known properties of RR Lyrae stars (see Table 1.3). The

Table 1.3: Fundamental data for RR Lyrae stars, adopted from Smith (1995).

Pulsation period	P	0.2 - 1.1 days
Mean V magnitude	$< M_v >$	+0.6±0.2 (metal poor)
Mean effective temperature	$< T_e >$	7400K - 6100K
Mean gravity	$<$ log g $>$	2.5 - 3.0
Metallicity	$[Fe/H]$	0.0 to - 2.5
Mass	M	$\approx 0.7 M_{\odot}$
Radius	R	4 - 6 $R_{\odot}$

surface temperatures of RR Lyrae stars are in the range of 7400K to 6100K. However, the hottest RR Lyrae stars are the type RRc of mean temperature $\sim$ 7400K and the coolest RR Lyrae stars are RRab $\sim$ 6100K.

RR Lyrae stars have got a range in chemical compositions. To characterise the overall heavy element abundance of stars, astronomers often employ the [Fe/H] notation. This notation means, the ratio of iron to hydrogen in the photosphere of one star is related to that ratio in another star, usually the sun: mathematically it can be written as; [Fe/H] = log(iron/hydrogen)$_{stars}$ - log(iron/hydrogen)$_{sun}$.

There are 5 different sub-type of RR Lyrae stars, classified by the appearance of their light curves, namely:

(i) RRa: Asymmetric light curves with a fast rise and slower decline. Radial fundamental mode pulsators;

(ii) RRb: Same as RRab type, but with smaller amplitude. Radial fundamental mode pulsators;

(iii) RRab: Often RRa and RRb are lumped together as RRab;

(iv) RRc: Nearly sinusoidal light curves with amplitudes $\sim$ 0.5 mag, radial first overtone pulsators;

(v) RRd: Refered to as "double mode" RR Lyraes, pulsating in the fundamental and

first overtone radial modes.

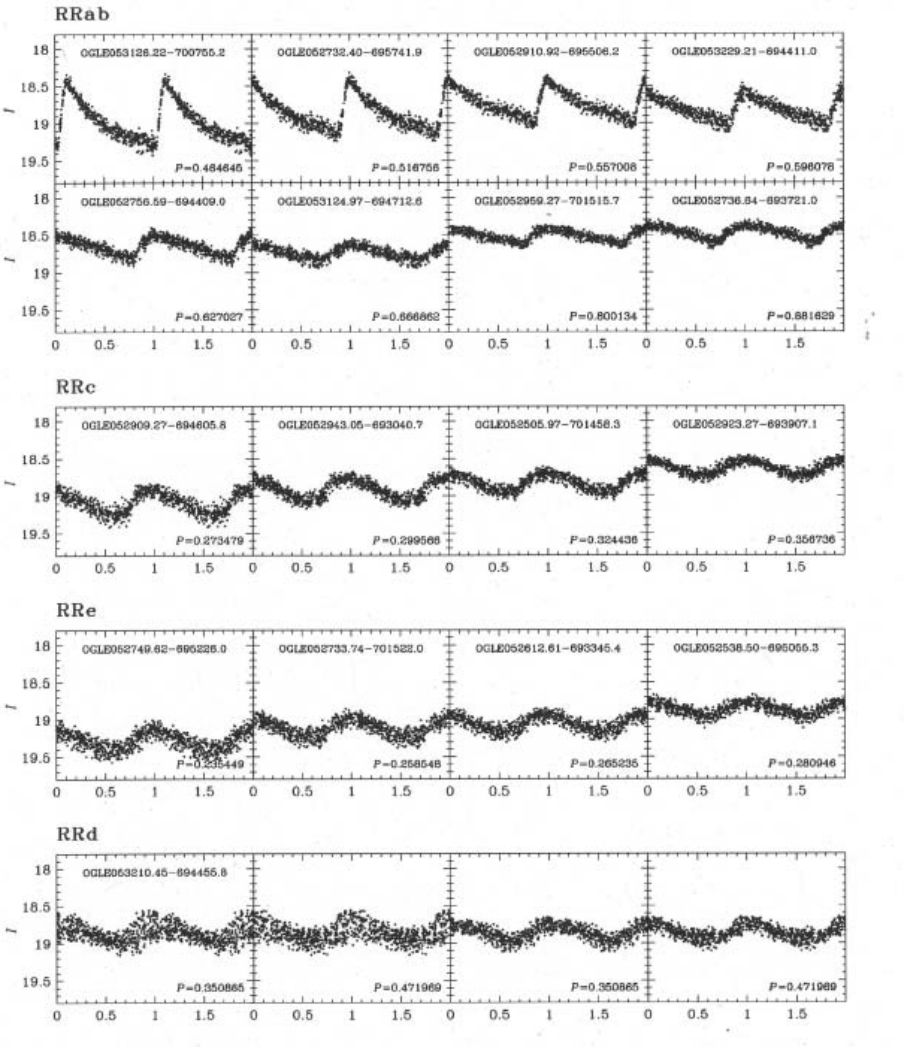

Figure 1.5: Exemplary light curves of RR Lyrae stars in the LMC. Adopted from Soszyński et al. (2003).

However, in addition to the above, some RR Lyrae stars show a modulation of the amplitude and shape of their light curves while their pulsation remain constant. This is refered to as the Blazhko effect and can be seen in Figure 1.6.

The importance of RR Lyrae stars in astrophysics is that they are used as tracers of chemical and dynamical properties of old stellar populations in galaxies, and in addition, they are also used as test objects for evolutionary and pulsation models of

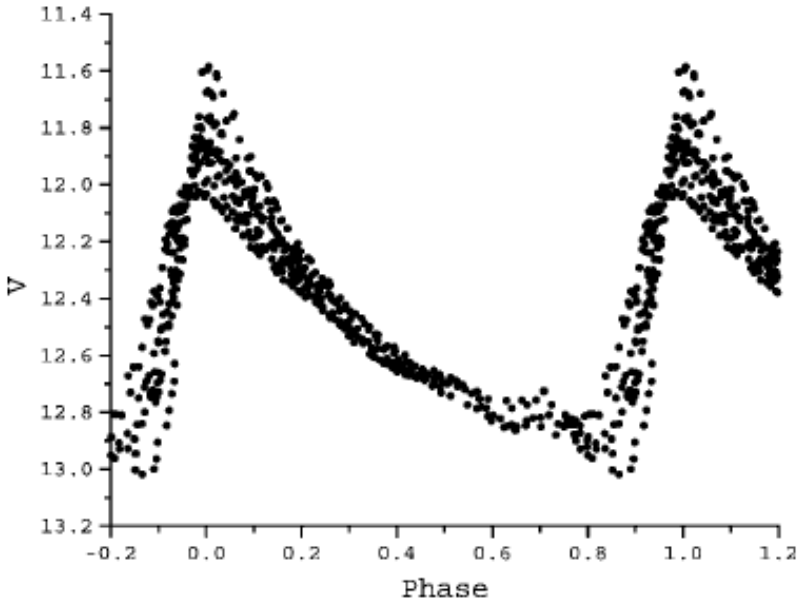

Figure 1.6: The Blazhko effect of the RR Lyrae star DR Andromedae. Adopted from Lee & Schmidt (2001).

low mass stars. The importance of OGLE III is that it was able to detect large samples of variable stars in the LMC compared to other surveys, i.e. $\sim$ 25000 RR Lyrae stars.

Chapter 2

Iron abundance from light curve shapes

2.1 Obtaining [Fe/H] from light curve shapes

Many authors have studied the relation between metallicity and period (e.g. Sandage, 1993; Layden, 1995; Sarajedini et al., 2006) and all have found that the metallicity of RRab stars increases as their period decreases (Figure 2.1). Smith (1995) gives a graphical relation between [Fe/H] and period for Galactic RR Lyrae stars. However, Jurcsik & Kovács (1996) later suggested that the best basic relation for Galactic RR Lyrae stars is given in terms of Fourier parameter φ_{31} and period, and that this relation gives less scatter. Jurcsik & Kovács (1996) method was for light curves of RRab stars in the V band for a sine decomposition.

Using the Galactic RR Lyrae data, Jurcsik & Kovács (1996) found

$$[Fe/H] = -5.038 - 5.394P + 1.345\varphi_{31}. \tag{2.1}$$

The Fourier parameters are defined as

$$\varphi_{21} = \varphi_2 - 2\varphi_1,$$

$$\varphi_{31} = \varphi_3 - 3\varphi_1.$$

Where φ_{21} and φ_{31} describe the phase differences between the second and the third terms and the leading term (Simon & Lee, 1981).

The aim in this section is to test Jurcsik & Kovács (1996) suggestion using the LMC

data (OGLE III data).

Using the available spectroscopically derived [Fe/H] values for LMC RR Lyraes from Gratton et al. (2004), we were able to match those stars with the corresponding ones in the OGLE III data base which had φ_{31} and period. It is important to point out that Di Fabrizio et al. (2005) provides us with the right ascension and declination and that, the φ_{31} values in the OGLE III data base was obtained from the light curves of stars in the I band for cosine decomposition. This was because most of the observations were done through the I band filter and therefore the light curves were better defined in I.

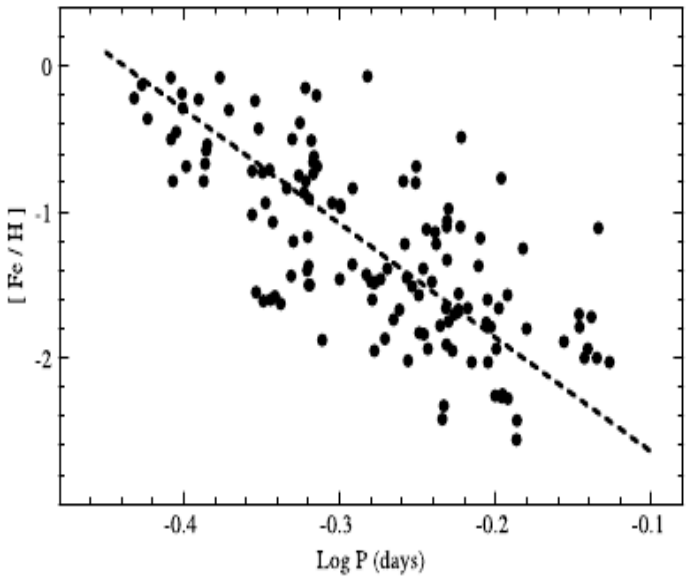

Figure 2.1: Metallicity - period relation, adopted from Sarajedini et al. (2006), showing how [Fe/H] of RRab stars increases as period decreases.

2.1.1 Method used in analysing the basic relation connecting [Fe/H], period and φ_{31}

Table 2.1 is for the data obtained from Gratton et al. (2004), Di Fabrizio et al. (2005) and OGLE III for our matched samples. We investigated the correlation between [Fe/H] with the OGLE period and also the correlation between [Fe/H], period and φ_{31} (OGLE III). This is because the I band light curves are better defined than those in V as just mentioned. We used the Maximum Likelihood method (see appendix) to search for the values of the coefficient of period, φ_{31} and the constant. The linear relation was of the

form:

$$[Fe/H] = \alpha P + \gamma, \tag{2.2}$$

and when we introduced φ_{31} then we have:

$$[Fe/H] = \alpha P + \beta\varphi_{31} + \gamma. \tag{2.3}$$

Using the maximum likelihood method we obtained:

$$[Fe/H] = -1.90P - 0.43, \sigma = 0.19, \tag{2.4}$$

and

$$[Fe/H] = -3.264P + 0.275\varphi_{31} - 0.351, \sigma = 0.17. \tag{2.5}$$

The linear fits of equations 2.4 and 2.5 are shown in Figure 2.2 and 2.3 respectively.

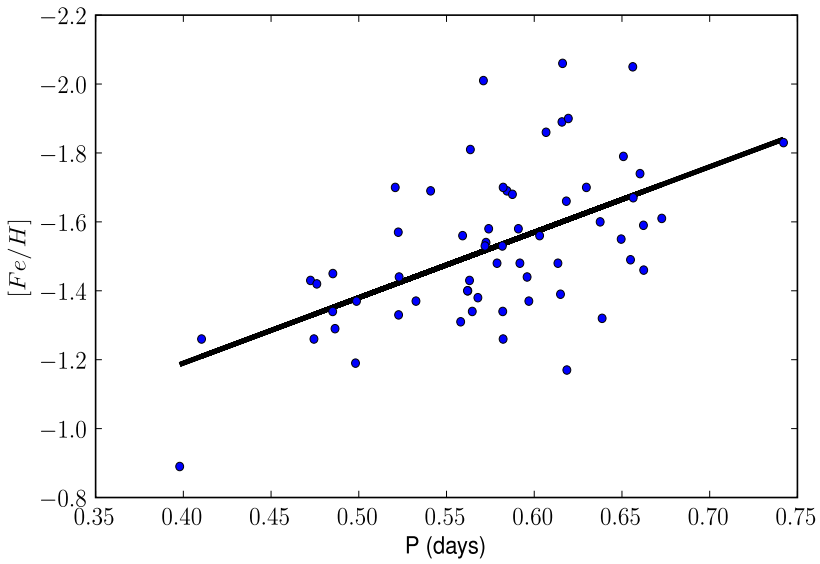

Figure 2.2: [Fe/H] vs period fitted with a line derived from equation 2.4.

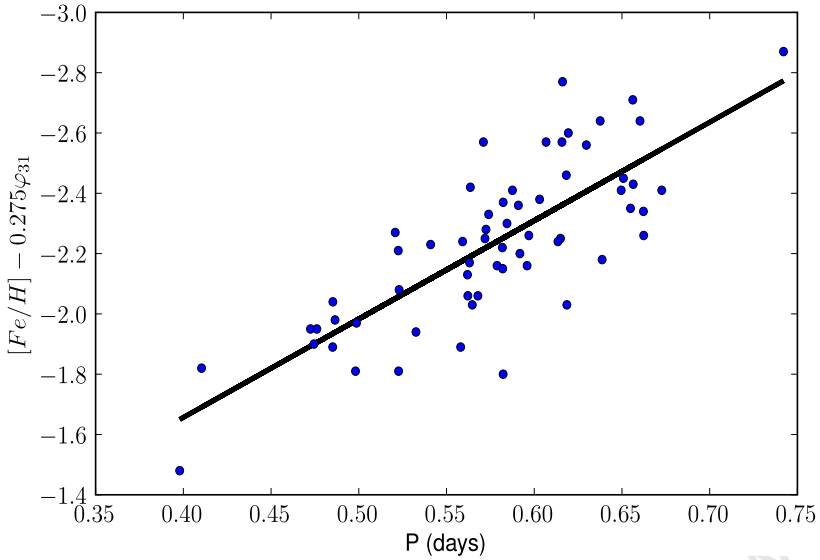

Figure 2.3: $[Fe/H] - 0.275\varphi_{31}$ vs period fitted with a line derived from equation 2.5.

2.1.2 Conclusion on [Fe/H], period and φ_{31} analysis

In testing the Jurcsik & Kovács (1996) suggestion, as indicated in equation 2.1, on the LMC data, we have found that introducing Fourier parameter φ_{31} in the [Fe/H]-period relation, did not improve on the relation without φ_{31} as seen in equation 2.4 and 2.5. The scatter around the formulae remained more or less the same with $\sigma = 0.19$ for [Fe/H]-period relation and $\sigma = 0.17$ when we introduced extra parameter φ_{31} (see equations 2.4 and 2.5). The slight decrease in σ in equation 2.5 can be attributed to the additional variable introduced. It is not possible to have a comparison between the published [Fe/H]-P-φ_{31} and the derived relationship since φ_{31} comes from V in one case and I in the other case, i.e. equation 2.1 and 2.5 respectively.

2.2 Metallicity, Period and Amplitude (A_V) relation

Alcock et al. (2000) showed that there exists a [Fe/H]-PA relation for Galactic Globular clusters RRab stars i.e.

$$[Fe/H] = -8.85 log PA - 2.60, \tag{2.6}$$

where PA is the reduced period and it is related to the RRab period P by:

$$logPA = logP + 0.15A_V, \tag{2.7}$$

and A_V is the amplitude in the V band. So we can write:

$$[Fe/H] = -8.85[logP + 0.15A_V] - 2.60, \sigma = 0.31. \tag{2.8}$$

2.2.1 Method in analysing the basic relation connecting [Fe/H], period and A_V

The aims in this section were to:

(i) derive a relation between [Fe/H] and logP;

(ii) derive a relation similar to equation 2.8, i.e. a relation connecting [Fe/H], logP and A_V using the same LMC data by searching for the coefficients of our parameters using the Maximum Likelihood method;

(iii) compare the scatter in (i) and (ii) and deduce which relation gives less scatter.

We used the selected LMC data in Table 2.1 to obtain the relation connecting [Fe/H] and logP, i.e.

$$[Fe/H] = -2.472logP - 2.125, \sigma = 0.19, \tag{2.9}$$

and for the case of [Fe/H], logP and A_V relation, we obtained:

$$[Fe/H] = -3.24logP - 0.294A_V - 2.05, \sigma = 0.18. \tag{2.10}$$

2.2.2 Conclusion on [Fe/H], period and A_V relation

Using the data from the LMC, we found out that introducing the light amplitude, A_V, in the [Fe/H]-logP relation did not improve on the formula. The scatter around the formulae remained more or less the same, with $\sigma = 0.19$ for the [Fe/H]-logP relation as seen in equation 2.9 and $\sigma = 0.18$ when we introduced extra parameter A_V as seen in equation 2.10. The scatter about equation 2.8 is much large.

2.3 General conclusion

The above results lead us to conclude that neither the introduction of φ_{31} or A_V improves the metallicity-period relation.

Star ID	RA (J2000)	Dec (J2000)	[Fe/H] Gratton	Period OGLE	φ_{31} OGLE	A_V DiFabrizio	A_I OGLE
7247	05 23 25.53	-70 32 33.45	-1.40	0.56215	2.397	0.714	0.375
7325	05 23 39.08	-70 32 24.81	-1.29	0.48645	2.492	1.131	0.736
7477	05 24 02.92	-70 32 08.60	-1.67	0.65641	2.775	1.108	0.744
7609	05 23 48.34	-70 32 00.33	-1.54	0.57250	2.681	0.788	0.556
8094	05 22 43.00	-70 31 23.70	-1.83	0.74207	3.784	0.452	0.321
8720	05 23 50.14	-70 30 16.73	-1.79	0.65082	2.395	1.163	0.697
8788	05 23 22.35	-70 30 14.64	-1.56	0.55917	2.462	0.939	0.657
9154	05 23 02.88	-70 29 44.63	-1.66	0.61829	2.897	0.662	0.395
9245	05 23 07.61	-70 29 36.50	-1.38	0.56788	2.469	0.706	0.499
9494	05 22 49.20	-70 29 13.50	-1.69	0.58446	2.201	1.150	0.752
19450	05 23 37.89	-70 34 06.71	-0.89	0.39792	2.144	1.344	0.943
25362	05 23 38.48	-70 30 08.55	-1.48	0.57879	2.490	1.078	0.610
26933	05 23 53.78	-70 28 59.71	-1.34	0.48512	1.994	1.188	0.699
28066	05 23 30.05	-70 28 11.07	-1.44	0.59593	2.610	0.496	0.453
6398	05 22 40.71	-70 33 50.18	-1.40	0.56195	2.638	0.883	0.561
6426	05 22 32.47	-70 33 48.73	-1.59	0.66224	2.736	1.045	0.687
7211	05 22 21.12	-70 32 43.96	-1.33	0.52269	1.750	0.875	0.474
7468	05 22 30.00	-70 32 20.56	-1.32	0.63869	3.141	0.492	0.287
7734	05 22 07.82	-70 31 59.83	-1.39	0.61496	3.130	0.502	0.332
10214	05 21 31.10	-70 28 12.01	-1.48	0.59182	2.613	0.633	0.352
10487	05 22 24.55	-70 27 40.52	-1.58	0.59096	2.829	0.913	0.620
25301	05 21 33.95	-70 30 24.47	-1.43	0.56311	2.709	1.005	0.562
25510	05 22 13.37	-70 30 11.50	-1.55	0.64955	3.129	0.609	0.336
6525	05 21 52.45	-70 29 28.68	-1.57	0.52250	2.330	0.863	0.718
26821	05 21 53.90	-70 29 17.47	-1.37	0.59692	3.241	0.752	0.457
28293	05 21 46.08	-70 28 13.20	-1.74	0.66029	3.288	0.403	0.229
3948	05 22 40.34	-70 37 16.96	-1.46	0.66238	2.920	0.959	0.547
4933	05 22 29.99	-70 35 53.61	-1.48	0.61349	2.755	0.793	0.510

Table 2.1: Matched stars from Di Fabrizio et al. (2005), Gratton et al. (2004) and Soszyński et al. (2009) - OGLE III.

Star ID	RA (J2000)	Dec (J2000)	[Fe/H] Gratton	Period OGLE	φ_{31} OGLE	A_V DiFabrizio	A_I OGLE
5589	05 22 09.54	-70 35 02.50	-1.60	0.63757	3.774	0.364	0.235
15387	05 21 30.38	-70 37 11.30	-1.81	0.56359	2.205	0.705	0.507
16249	05 22 08.22	-70 36 31.00	-1.86	0.60674	2.569	1.118	0.634
19711	05 22 38.14	-70 34 02.02	-1.69	0.54094	1.970	0.961	0.639
2525	05 23 32.39	-70 39 15.34	-2.06	0.61615	2.583	0.991	0.654
2767	05 23 17.70	-70 38 55.9	-1.37	0.53259	2.073	1.091	0.528
3061	05 23 25.13	-70 38 28.94	-1.26	0.47444	2.343	0.809	0.575
4974	05 22 51.21	-70 35 47.69	-1.34	0.58204	2.957	0.764	0.514
12896	05 22 46.09	-70 38 54.95	-1.53	0.57193	2.623	0.911	0.590
18314	05 22 49.08	-70 34 59.12	-1.68	0.58757	2.657	1.120	0.688
7063	05 18 43.98	-70 55 55.77	-1.49	0.65487	3.111	0.633	0.387
7620	05 18 03.53	-70 55 03.12	-2.05	0.65616	2.413	1.071	0.648
22917	05 18 19.05	-70 54 56.03	-1.34	0.56468	2.513	0.957	0.616
23502	05 18 01.58	-70 54 31.81	-1.43	0.47247	1.888	1.296	0.852
24089	05 17 44.64	-70 54 03.08	-1.31	0.55806	2.099	0.371	0.492
4780	05 16 53.00	-71 00 02.53	-1.17	0.61859	3.119	0.595	0.365
4859	05 16 10.87	-70 59 54.34	-1.44	0.52298	2.338	1.061	0.680
5902	05 16 12.23	-70 58 04.86	-2.01	0.57103	2.039	1.015	0.672
6020	05 16 32.44	-70 57 53.68	-1.89	0.61579	2.459	0.858	0.503
6440	05 16 16.68	-70 57 11.56	-1.19	0.49813	2.266	0.875	0.671
6798	05 17 11.33	-70 56 32.65	-1.26	0.58226	1.974	1.035	0.353
7442	05 17 15.68	-70 55 26.77	-1.58	0.57403	2.726	0.650	0.298
19037	05 16 20.66	-70 58 06.31	-1.26	0.41038	2.031	1.466	0.977
1408	05 17 13.79	-71 06 06.91	-1.70	0.62971	3.122	0.812	0.515
1575	05 16 31.27	-71 05 48.49	-1.61	0.67268	2.927	1.029	0.601
2055	05 17 17.39	-71 04 50.18	-1.70	0.52077	2.058	0.749	0.330
2249	05 17 13.01	-71 04 27.10	-1.56	0.60306	2.986	0.747	0.467
2884	05 16 52.13	-71 03 25.18	-1.90	0.61943	2.545	0.869	0.609
3400	05 17 14.46	-71 02 26.58	-1.45	0.48521	2.149	1.263	0.905
14449	05 17 05.32	-71 01 40.85	-1.70	0.58229	2.441	0.804	0.562
1907	05 18 12.30	-71 04 59.49	-1.53	0.58183	2.493	0.658	0.546
3033	05 18 13.98	-71 03 00.56	-1.37	0.49870	2.173	1.157	0.538
10811	05 18 15.95	-71 04 27.07	-1.42	0.47608	1.933	1.166	0.563

Table 2.1. Continued.

2.4 Optical Gravitational Lensing Experiment III (OGLE III)

2.4.1 Description of the survey

Observations of variable stars in the LMC were made by the OGLE III survey which lists 24906 RR Lyrae stars (Soszyński et al., 2009). Out of the total number of RR Lyrae stars, OGLE III detected 17693 fundamental-mode (RRab), 4958 first-overtone (RRc), 986 double-mode (RRd) and 1269 second-overtone (RRe) pulsators. The OGLE III survey in the LMC covered nearly 40 square degrees that were divided up into 116 fields, each marked with identification numbers starting from 100 to 215 as shown in Figure 2.4.

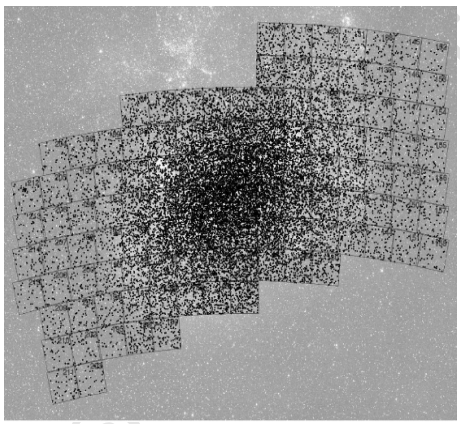

Figure 2.4: The distribution of RR Lyrae stars, adopted from Soszyński et al. (2009).

Between July 2001 and March 2008, approximately 400 photometric points per star were accumulated over seven seasons. The OGLE III observations were carried out with the 1.3-m Warsaw telescope located at Las Campanas Observatory, Chile. The telescope has a camera which uses 2048 × 4096 CCD detectors with 15 μm pixel and a $35' \times 35'.5$ field of view (Udalski et al., 2003).

Figure 2.5: Left: The telescope and its CCD camera. Right: Control building and the dome (Adopted from http://ogle.astrouw.edu.pl/main/tel.html).

2.5 Methods for analysing the OGLE III data

2.5.1 Analysis of fundamental mode RR Lyrae stars (RRab)

We started with 17693 fundamental-mode (RRab), however, one star with the name OGLE-LMC-RRLYR-15485 has been found to have no LMC field number. This leaves us with a total of 17692 RRab stars, out of which we removed all those stars which were classified as uncertain type, foreground stars, Galactic RR Lyrae. This leaves us with a total of 17296 in our sample and at this stage we had to carry out the analysis in two different ways; **part A**-samples when the bright stars removed, **part B**-samples containing the bright stars. The reason for removing the bright stars in our sample was because we were not sure whether those were normal LMC RR Lyrae stars (i.e. they could have blended and foreground stars). However, it is important to point out that the globular clusters in which RRab stars were found have been marked by Soszyński et al. (2009) as shown in Table 2.4 and were removed from our samples-see Figure 2.6 and 2.7.

Cluster name	RA (J2000)	Dec (J2000)	Cluster radius [′]	N_{ab}
NGC 1754	$4^h54^m17^s$	-70° 26′29″	1.6	20
NGC 1786	$4^h59^m06^s$	-67° 44′42″	2.0	28
NGC 1835	$5^h05^m06^s$	-69° 24′14″	2.3	63
NGC 1898	$5^h16^m41^s$	-69° 39′23″	1.6	31
NGC 1916	$5^h18^m38^s$	-69° 24′23″	2.1	15
NGC 1928	$5^h20^m57^s$	-69° 28′40″	1.3	7
NGC 1939	$5^h21^m26^s$	-69° 56′59″	1.4	3
NGC 2005	$5^h30^m10^s$	-69° 45′10″	1.6	9
NGC 2019	$5^h31^m56^s$	-70° 09′33″	1.5	36
NGC 2210	$6^h11^m31^s$	-69° 07′18″	3.3	34

Table 2.2: LMC Globular Clusters in which RRab stars were found.

2.6 Part A-samples with the bright stars removed (16864)

In this part of our analysis, we applied a cutoff to the data by removing all stars whose I < 18.3 mag. From 17296 RRab stars in our original sample, after applying our cutoff limit we were left with 16864 RRab stars.

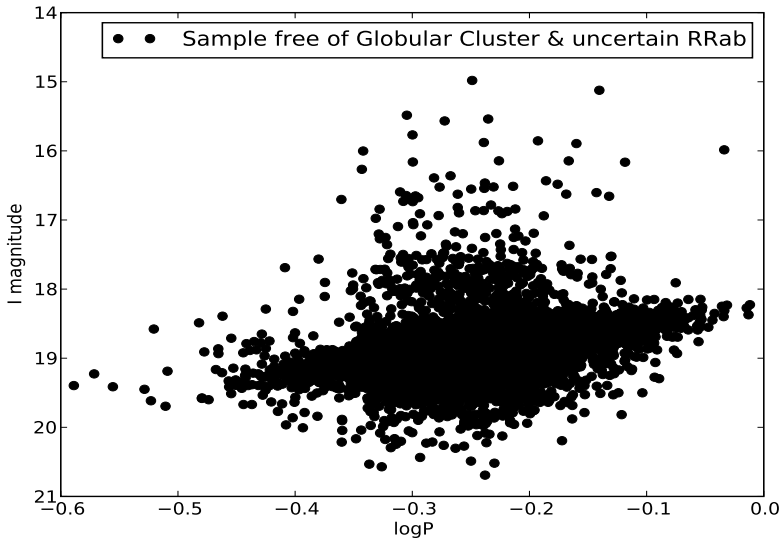

Figure 2.6: The sample containing the bright stars.

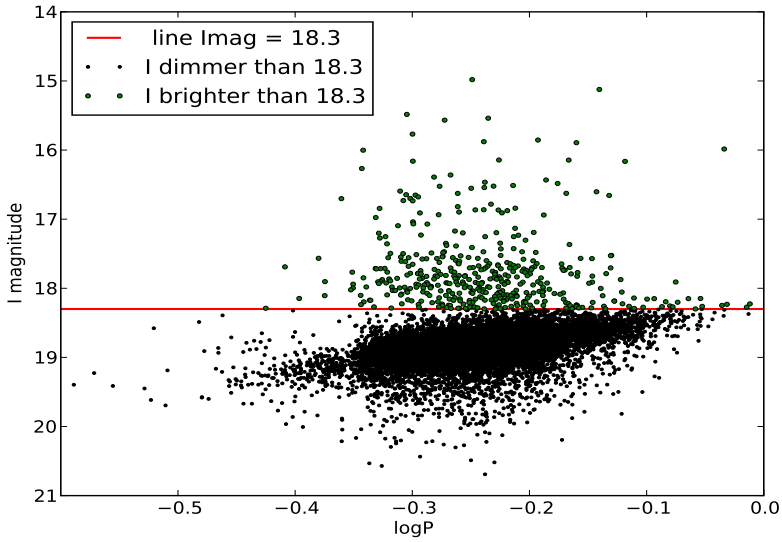

Figure 2.7: Plot used for removing the bright and foreground RRab stars from our original sample, i.e. RRab stars with I $<$ 18.3 mag which we used in analysis for part A.

Chapter 3

Iron abundance and galactocentric distance-selection according to model

Cioni (2009) adopts a model for the LMC which is that of a disc inclined to the plane of the sky. However, the true three dimensional distribution of RR Lyraes in the LMC is not at present known and we follow the model adopted by Cioni (2009) as a first approximation. This adopts an inclination i = 34.7°, a position angle of the major axis PA = 189.3° and an LMC distance D = 51 kpc. Cioni (2009) distance is adopted so that a direct comparison can be made with her results.

We also adopted the method of Van Der Marel & Cioni (2001) in transforming the (RA, Dec) to (X, Y) cartesian coordinate system. Using this model we determined the distance R_{RG} of each RRab star in our final OGLE sample from the centre of the LMC, taken with Cioni as $\alpha = 82.25°$ and δ = -69.5°, while the iron abundance [Fe/H] of each star in our OGLE sample (**section 2.5, part A**) was calculated from a logP-[Fe/H] relation based on the data of A. C. Layden (2005, private communication).

3.1 Calculation of galactocentric distance

3.1.1 Angular coordinate

The theoretical framework of the calculation of angular coordinate is adopted from the work of Van Der Marel & Cioni (2001). The position of any point in space is determined by its RA and Dec on the sky, (α, δ) and its distance D. A particular point O with

coordinates (α_o, δ_o, D_o) is taken to be the origin of the analysis. In this case, the point O is taken to be the centre of the LMC.

Angular coordinates (ρ, ϕ) are defined on the celestial sphere, where ρ is the angular distance between the points (α, δ) and (α_o, δ_o), and ϕ is the position angle of the point (α, δ) with respect to (α_o, δ_o). By convention, ϕ is measured counterclockwise starting from the axis that runs in the direction of decreasing RA at constant declination δ_o.

The cosine rule of spherical trignometry (e.g., Smart 1977) can be used to derive

$$cos\rho = cos\delta cos\delta_o cos(\alpha - \alpha_o) + sin\delta sin\delta_o. \tag{3.1}$$

However, the sine rule of spherical trignometry can also be used to show that

$$sin\rho cos\phi = -cos\delta sin(\alpha - \alpha_o), \tag{3.2}$$

and from where the so-called analog formular implies that

$$sin\rho sin\phi = sin\delta cos\delta_o - cos\delta sin\delta_o cos(\alpha - \alpha_o). \tag{3.3}$$

The above formlae define (ρ, ϕ) as a function of (α, δ) for a fixed choice of the origin O. The most important information to note is that it is often useful to plot observations from the celestial sphere on a flat piece of paper. This calls for transformation from (α, δ) to a cartesian coordinate system (X, Y), which are given by:

$$X(\alpha, \delta) = \rho cos\phi, \tag{3.4}$$

$$Y(\alpha, \delta) = \rho sin\phi. \tag{3.5}$$

Equations 3.4 and 3.5 are the so-called zenithal equidistant projection which provides one of the many possible ways of projecting a sphere onto a plane.

3.1.2 Galactocentric distance

Having obtained X and Y, i.e. equations 3.4 and 3.5, we then followed the method of Cioni (2009) for calculating galactocentric distance as described below.

We rotated the coordinate system according to:

$$X_1 = X \times cos(\theta) + Y \times sin(\theta), \tag{3.6}$$

$$Y_1 = Y \times cos(\theta) - X \times sin(\theta), \tag{3.7}$$

This is followed by de-projection given by:

$$Y_2 = Y_1/cos(i), \tag{3.8}$$

and calculating the angular distance and later converting into kpc with

$$d_{deg} = \sqrt{{X_1}^2 + {Y_2}^2}, \tag{3.9}$$

$$d_{kpc} = D \times tg(d), \tag{3.10}$$

where θ = PA - 90° (See Cioni (2009), Van Der Marel & Cioni (2001) for detail.)

3.1.3 Iron abundance [Fe/H] calculation

In the following subsections we estimate and discuss the [Fe/H] for the OGLE LMC RR Lyrae variables using their periods and a logP-[Fe/H] relation derived from Galactic RR Lyraes. A Galactic relation was used rather than an LMC one because the LMC RR Lyraes with spectroscopic abundances have limited range in [Fe/H], they are small in number and have substantial intrinsic scatter in logP at a given metallicity which preclude any attempt to derive an independent slope to the relation.

Figure 3.1 is a plot which shows the relation between period and metallicity for Galactic RRab stars. The data were kindly provided to us by Dr A. Layden. Plotted in Figure 3.1 is also spectroscopic values of [Fe/H] derived by Gratton et al. (2004) and Borissova et al. (2006) for the LMC. Two lines are shown in Figure 3.1, the dashed line is a Least Square Fit to the Layden data which has a relation given by:

$$[Fe/H] = -5.62(\pm 0.47)logP - 2.81(\pm 0.13), \sigma = 0.42, \tag{3.11}$$

and the solid line is given by

$$[Fe/H] = -7.82logP - 3.43, \sigma = 0.45. \tag{3.12}$$

Equation 3.12 is the relation used by Sarajedini et al. (2006) for an investigation

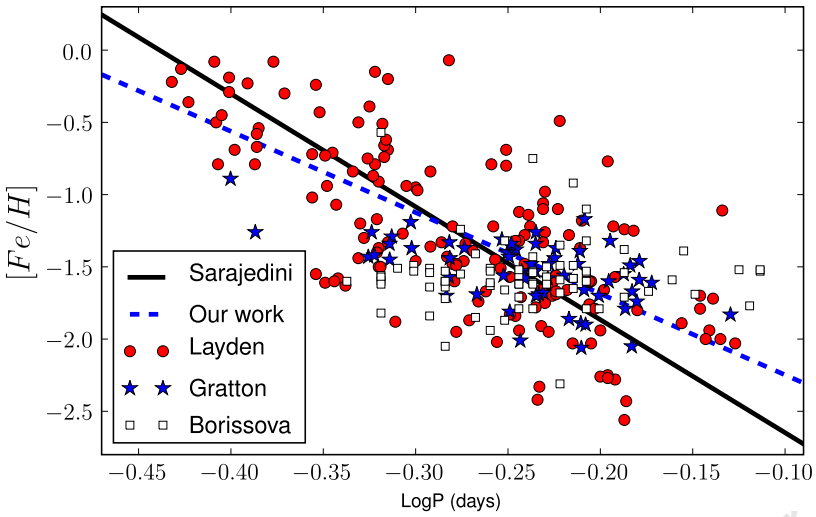

Figure 3.1: The relation between [Fe/H] and logP for Galactic RR Lyraes (circles from Layden) and LMC RR Lyraes (stars from Gratton and squares from Borissova) the lines are for equation 3.11 (dashed) and equation 3.12 (solid).

similar to the present one and is based on a slightly different sample of Galactic RRab stars which was supplied to them by Dr A. Layden. Sarajedini et al. (2006) used their relation for similar work on RR Lyraes in M33. Looking at Figure 3.1, Galactic data show a clear trend though with considerable scatter, while the LMC data from Gratton et al. (2004) and Borissova et al. (2006) generally lie together with the Galactic points. We therefore assume that the LMC RRab stars follow the Galactic relation and discuss the effect of possible deviations in **subsection 3.2.1**. We tested for the suggestions on the idea of improved relation involving both period and light-curve shape for estimating metallicity as seen in Chapter 2 and found no improvement in those cases (one of the reasons why 3.11 and 3.12 were chosen than 2.9). Our analysis is therefore based on equations 3.11 and 3.12.

3.1.4 Weighted Least Square Straight Line Fitting (WLSSLF)

In order to fit a line through data points which have different errors, one has to apply the Weighted Least Square Straight Line Fitting (WLSSLF). This is a method where one gives the least amount of weight to points that are the least reliable. This is attained

statistically by weighting each point by the inverse square of its standard error when calculating the best-fit slope and the intercept. We adopted the method of calculating the Weighted Least Square Straight Line Fitting as explained by Bevington (1969) page 106 - 107.

This is first done by establishing the standard error of each point and this quantity is called e_i which is pressumed to reside with y_i.

Therefore, for the weighted linear regression, the best fit values of the slope **a** and intercept **b** are then given by:

$$Slope = \frac{\left(\sum \frac{x_i}{e_i^2}\right)\left(\sum \frac{y_i}{e_i^2}\right) - \left(\sum \frac{x_i y_i}{e_i^2}\right)\left(\sum \frac{1}{e_i^2}\right)}{\left(\sum \frac{x_i}{e_i^2}\right)^2 - \left(\sum \frac{x_i^2}{e_i^2}\right)\left(\sum \frac{1}{e_i^2}\right)} \tag{3.13}$$

$$Intercept = \frac{\left(\sum \frac{x_i}{e_i^2}\right)\left(\sum \frac{x_i y_i}{e_i^2}\right) - \left(\sum \frac{y_i}{e_i^2}\right)\left(\sum \frac{x_i^2}{e_i^2}\right)}{\left(\sum \frac{x_i}{e_i^2}\right)^2 - \left(\sum \frac{x_i^2}{e_i^2}\right)\left(\sum \frac{1}{e_i^2}\right)} \tag{3.14}$$

The uncertainities in the slope and the intercept of a WLSSLF that was weighted by the individual errors of the points are given by ;

$$Slope_{error} = \sqrt{\frac{\sum \frac{1}{e_i^2}}{\left(\sum \frac{x_i^2}{e_i^2}\right)\left(\sum \frac{1}{e_i^2}\right) - \left(\sum \frac{x_i}{e_i^2}\right)^2}} \tag{3.15}$$

$$Intercept_{error} = \sqrt{\frac{\sum \frac{x_i^2}{e_i^2}}{\left(\sum \frac{x_i^2}{e_i^2}\right)\left(\sum \frac{1}{e_i^2}\right) - \left(\sum \frac{x_i}{e_i^2}\right)^2}} \tag{3.16}$$

3.1.5 Analysis and results for iron abundance & galactocentric distance

We started by obtaining a plot of [Fe/H] vs galatocentric distance for all our final OGLE III as in **section 2.5, part A**. The aim here was to choose annuli with large enough numbers of stars based on the galactocentric distance distribution. The sample was divided up into twelve different groups based on Figure 3.2 and the results were tabulated as seen in Table 3.1 and 3.2. We obtained the average values of the iron abundance ([Fe/H]) and galactocentric distance for all the stars in the different groupings (bins) using either equation 3.11 or 3.12.

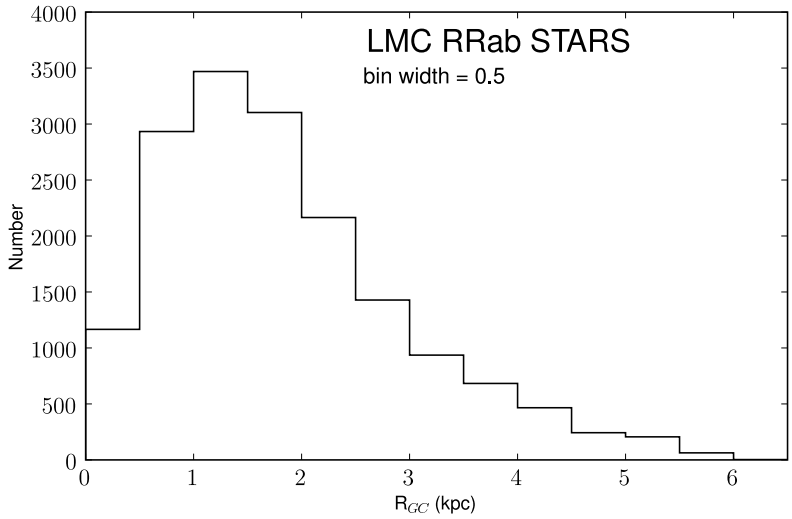

Figure 3.2: The galactocentric distance distribution of RRab stars in our final sample.

Table 3.1: The various grouping of RRab stars obtained using the histogram in Figure 3.2 for the [Fe/H] values obtained using equation 3.11.

Mean R_{GC} (kpc)	Mean $[Fe/H]_{Cal}$	Standard deviation of the mean [Fe/H]
0.33	-1.420	0.009
0.77	-1.432	0.006
1.25	-1.432	0.005
1.74	-1.443	0.006
2.23	-1.442	0.006
2.75	-1.453	0.008
3.24	-1.462	0.010
3.74	-1.448	0.012
4.24	-1.460	0.014
4.73	-1.490	0.018
5.24	-1.476	0.022
5.68	-1.438	0.037

Table 3.2: The various grouping of RRab stars obtained using the histogram in Figure 3.2 for the [Fe/H] values obtained using equation 3.12.

Mean R_{GC} (kpc)	Mean $[Fe/H]_{Cal}$	Standard deviation of the mean [Fe/H]
0.33	-1.495	0.012
0.77	-1.513	0.008
1.25	-1.512	0.007
1.74	-1.528	0.008
2.23	-1.527	0.009
2.75	-1.541	0.011
3.24	-1.554	0.014
3.74	-1.534	0.017
4.24	-1.551	0.020
4.73	-1.593	0.025
5.24	-1.574	0.031
5.68	-1.521	0.051

The result in Table 3.1 and 3.2 were plotted in Figure 3.3, we applied the Weighted Least Squares Straight Line Fitting (WLSSLF) to the data where the slope and intercept were obtained. We found a gradient given by

$$[Fe/H] = -0.015(\pm 0.003) \times R_{GC} - 1.498(\pm 0.006), \tag{3.17}$$

which is obtained from the relation of Sarajedini et al. (2006) and

$$[Fe/H] = -0.010(\pm 0.002) \times R_{GC} - 1.421(\pm 0.005) \tag{3.18}$$

from our relation as seen in Figure 3.3.

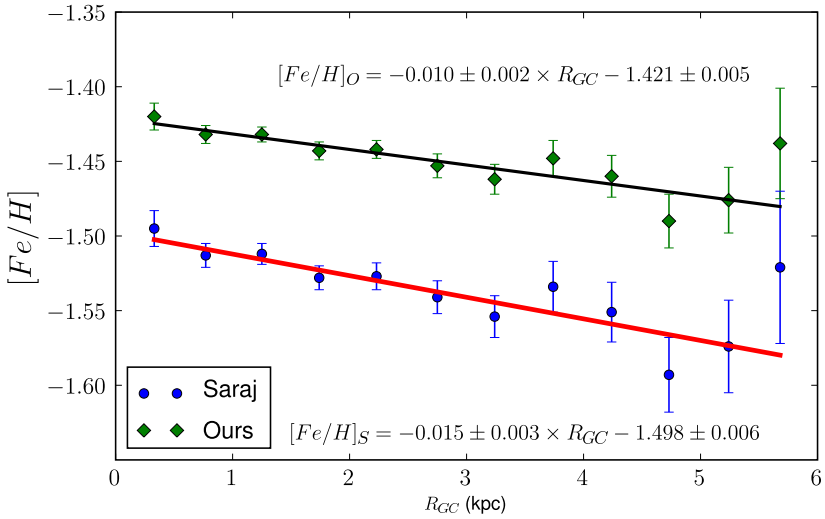

Figure 3.3: The mean [Fe/H] shown against R_{GC} and fitted with a line obtained using Weighted Least Square Straight Line Fitting. $[Fe/H]_O$ is the values obtained from our relation while $[Fe/H]_S$ is obtained from the Sarajedini et al. (2006) relation.

3.1.6 Conclusion on [Fe/H]-period relation

From the analysis of [Fe/H]-period relation for the RRab stars, we established a small but significant mean metallicity gradient in the LMC as seen in equation 3.17 and 3.18. The two equations give nearly equal gradients and the absolute values of the metallicities differ by less than the standard error of the zero-point in equation 3.11.

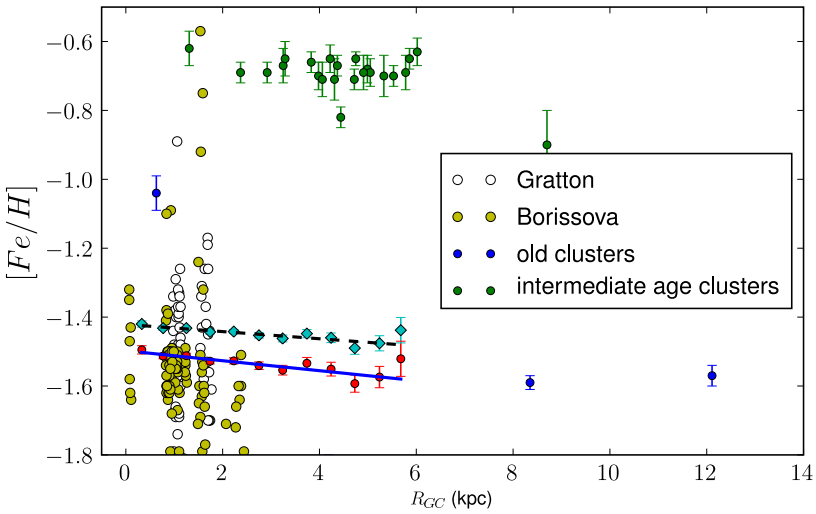

Figure 3.4: Blue and green points with error bars are the LMC stellar clusters taken from table 1 and table 4 of Grocholski et al. (2006) with metallcity conversion from Cioni (2009) equation A1 in appendix. Open circle are the spectroscopic [Fe/H] of RR Lyrae from Gratton et al. (2004), while yellow filled circles are the spectroscopic [Fe/H] of RR Lyrae from Borissova et al. (2006). Points fitted with solid blue and dashed lines are those in our studies. The stellar cluster ages were estimated based on the SWB Type.

3.1.7 Discussion and interpretation of the analysis on [Fe/H] and R_{GC}

Cioni & Habing (2003) selected stars from the DENIS survey of the LMC with luminosity above the tip of the Red Giant Branch (RGB) and used IJK magnitudes and colours to distinguish between probable AGB carbon (C -type) and AGB stars of class M0+ (oxygen rich stars of type later than M0) and finally studied the variation of the C/M0+ ratio in the LMC. This was followed by the work of Battinelli & Demers (2005) who obtained a relationship for estimating [Fe/H] from the C/M0+ ratio. The relationship is given by:

$$[Fe/H] = -1.32(\pm 0.07) - 0.59(\pm 0.09) \times log(C/M0+). \tag{3.19}$$

Cioni (2009) later on carried out studies on the stellar metallicity and its gradient in the LMC by making use of the AGB stars, and estimating [Fe/H] from the C/M0+ using equation 3.19. The result obtained by Cioni (2009) is that the metallicity of the

LMC decreases linearly as -0.047±0.003 dex kpc^{-1} out to $\sim$ 8 kpc from the centre and our result indicates that the metallicity decreases with distance as -0.015±0.003 dex kpc^{-1} and -0.010±0.002 dex kpc^{-1} as seen in Figure 3.3 and equation 3.17 & 3.18.
As can be seen the gradient obtained by Cioni (2009) and in our work are not the same. This could possibly be because of the different methods or approaches employed as can be further explained as follows:

1. Cioni (2009) used the fact that [Fe/H] depends on C/M0+ and this could possibly account for the differences in the gradient.
2. The fact that we used different LMC populations (objects), i.e. RR Lyrae stars rather than AGB stars could also account for the differences in the gradient.

In general, it is well known that the RR Lyrae stars are older than the AGB stars.
Pagel et al. (1978) studied the HII region abundances in the LMC by looking at oxygen abundance within 4 kpc of the LMC centre. They found out that there was marginal evidence of a radial gradient d log(O/H)/dR = -0.03±0.02/kpc in the LMC (see Figure 3.5). Grocholski et al. (2006) obtained abundances in the LMC for clusters and their result shows no evidence of a gradient-see Figure 3.4.

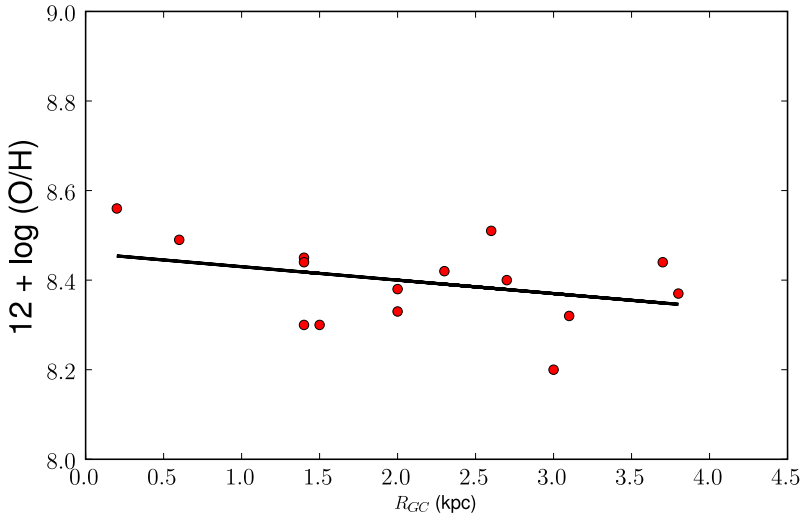

Figure 3.5: HII region abundance in the LMC, data taken from Pagel et al. (1978) table 9 (a). The Least Square Solution being given by 12 + log(O/H) = (-0.03±0.02)R$_{GC}$ - 8.46±0.06 and σ = 0.09 for 15 observations.

3.2 [Fe/H] for all RR Lyrae stars from Borissova and Gratton surveys

We obtained all the RR Lyrae stars with known spectroscopic [Fe/H] values from the Borissova survey (Borissova et al., 2006) - 103 stars and the Gratton survey (Gratton et al., 2004) - 98 stars. In total we gathered 201 RR Lyrae stars. The aim was to obtain as many RR Lyrae with known [Fe/H] as possible, so as to calculate the R_{GC} for each star and compare the gradient values with that of our previous work. The galactocentric distance of each star from the LMC centre was calculated using the models of Cioni (2009) and Van Der Marel & Cioni (2001). We later on applied the Least Square Straight line Fitting technique to the data ([Fe/H] and R_{GC}) as seen in Figure 3.6. We obtained the slope and intercept given by:

$$[Fe/H] = -0.050(\pm 0.037) \times R_{GC} - 1.480(\pm 0.045), \sigma = 0.18. \tag{3.20}$$

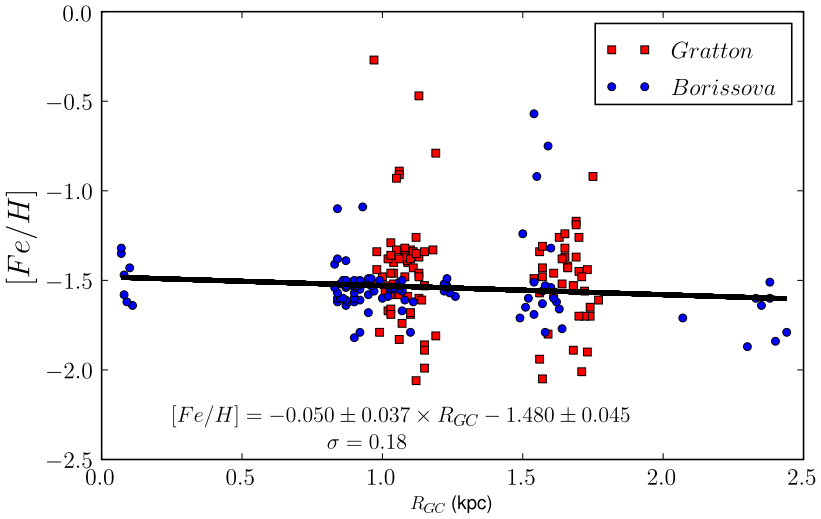

Figure 3.6: The spectroscopic [Fe/H] against R_{GC} fitted with a line obtained using Least Squares Straight Line Fitting.

3.2.1 Comparision of the metallicity gradients

Equation 3.17 and 3.18 give nearly equal gradients. They were obtained from the assumption that the LMC stars follow the [Fe/H]-period relation for Galactic stars.

The absolute values of their metallicities differ by less than the standard error of the zero-point in equation 3.11. Equation 3.20 was obtained from the LMC RR Lyraes with spectroscopically determined [Fe/H] from Gratton et al. (2004) and Borissova et al. (2006). The result obtained in equation 3.20 agree in slope and zero-point with those from the period distribution within the uncertainties, though the slope taken by itself, does not provide a convincing evidence of a metallicity gradient. Fitting a line through the LMC RR Lyraes with spectroscopically determined metallicity in Figure 3.1 would produce a shallower slope to the [Fe/H]-period relation than the Galactic stars and thus a shallower [Fe/H]-R_{GC} relation. However, we attribute this result to the narrow range of [Fe/H] values in the spectroscopic sample which come from the inner part of the LMC. In view of this, we assume that the LMC OGLE III RRab stars follow the Galactic relation.

3.3 Checking for blending

The longer period RRab stars are on average more metal poor and also of lower light amplitude than the shorter period ones. One might therefore be concerned that the results obtained and discussed above could be affected by a lower efficiency of finding low amplitude variables in the more crowded regions of the LMC. We have made attempts to check whether this is a significant effect by:

1. making a plot of amplitude-period relation,
2. determining the ratio of the number of RRab to RRc stars as a function of distance, R_{GC}, from the LMC centre.

3.3.1 Amplitude-period relation

We made a plot of amplitude-period relation, i.e. a plot of I-band amplitude vs log period (Figure 3.7) for three different cases, i.e. the inner, intermediate and outer fields. We found out that the RRab stars in all the three cases followed the same trend in the amplitude-period plots. In other words, if we were losing the long period stars at the LMC centre, we expect not to find long period RRab stars of small amplitude in

the inner or dense field. The fact that we observed similar trend in the three plots in Figure 3.7 suggests that we were not losing the long period RRab at the LMC centre.

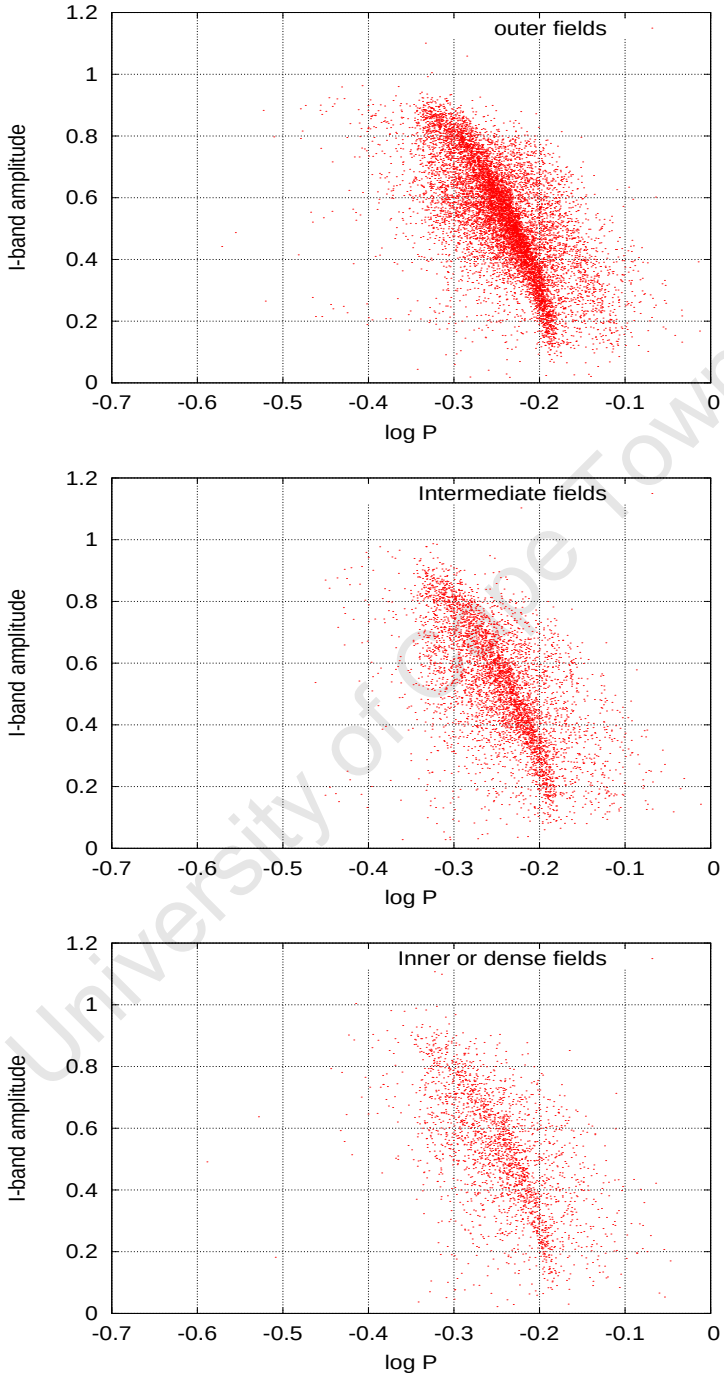

Figure 3.7: Plots used for checking for blending and other conterminations in the selected RRab stars.

3.3.2 Ratio of RRab to RRc analysis

We calculated the ratio of RRab to RRc stars as a function of distance, R_{GC}, from the centre. The RRc variables are of lower amplitude than the RRab stars. Thus, other things being equal, a selection effect should show as an increase of the N(ab)/N(c) ratio (loss of RRc variables) in the inner parts. Figure 3.9 shows no evidence of this, suggesting that we were not losing long period stars at the LMC centre.

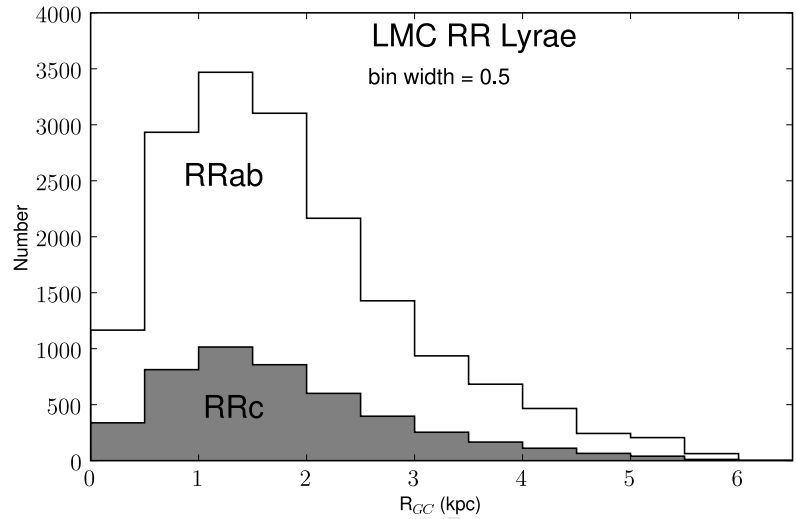

Figure 3.8: The galactocentric distance distribution for both RRab and RRc.

The data obtained from the histogram in Figure 3.8 is as shown in Table 3.3.

Table 3.3: The various grouping of RRab and RRc stars obtained using the histogram in Figure 3.8.

Mean R_{GC} (kpc)	Ratio of RRab to RRc	Error in the ratio
0.33	3.46	0.21
0.77	3.64	0.14
1.25	2.87	0.10
1.74	4.60	0.20
2.23	3.63	0.17
2.75	3.62	0.21
3.24	3.66	0.26
3.74	4.11	0.13
4.24	4.12	0.44
4.73	3.78	0.53
5.24	5.18	0.91
5.68	5.33	1.68

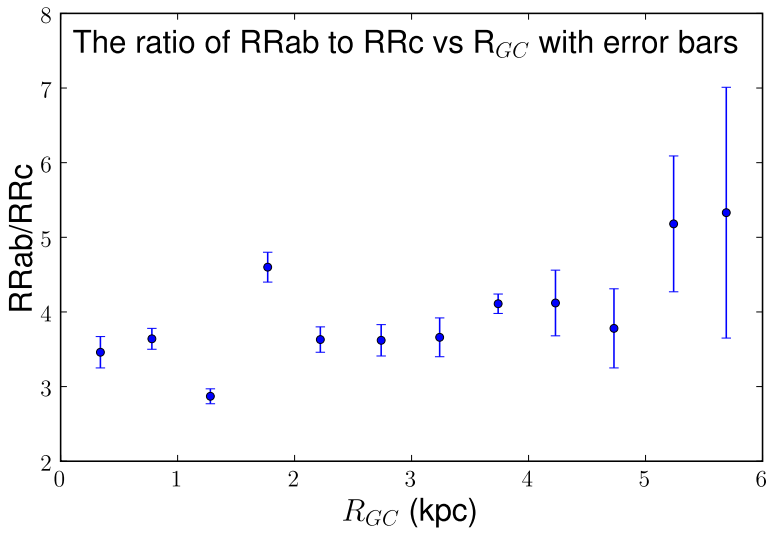

Figure 3.9: The ratio of RRab to RRc against Galactocentric distance with the error bars.

Chapter 4

Further test on metallicity gradient

4.1 Selection according to space density

Figure 4.1 is a histogram showing the period distribution of the RRab sample. Evidently most of the RRab stars are of intermediate period. In this section we examined the ratio of long period to short period RRab stars as a function of distance from the centre of the LMC, leaving out the stars of intermediate period. We might expect that this ratio would be somewhat more sensitive to a change in mean metallicity between regions than the mean period of regions for [Fe/H]-period relation. The data was analysed in two slightly different ways, i.e **part A**-samples when the bright stars removed and **part B**-samples containing the bright stars. The data were combined into three and five groupings defined by the number of our stars in each of the OGLE III fields with the aid of Figure 4.2 and the criteria used are indicated in Table 4.1 for the three groupings and Table 4.2 for the five groupings depending on the total number of RR Lyrae stars (N_T) for the bins. These groups are roughly concentric about the densest region. Their mean distances from the densest region is shown in Figure 4.3 and Figure 4.4 respectively. The selection of long period and short period stars was done in three different ways which we called cases as indicated in Table 4.3 for **part A** and Table 4.11 for **part B**. The ratios are plotted against region numbers (1 the most dense, 3 the least dense for three groupings & 5 least dense for five groupings). For the five groupings in the three different cases, least square fits are shown. This was followed by testing for the significance differences in the period distribution amongst the different regions (fields) in our groupings using the χ^2 test.

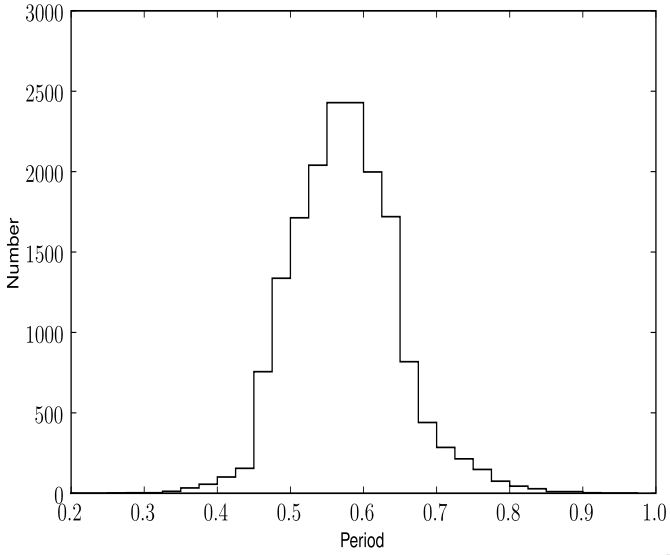

Figure 4.1: The histogram showing period distribution of selected RRab stars in our sample.

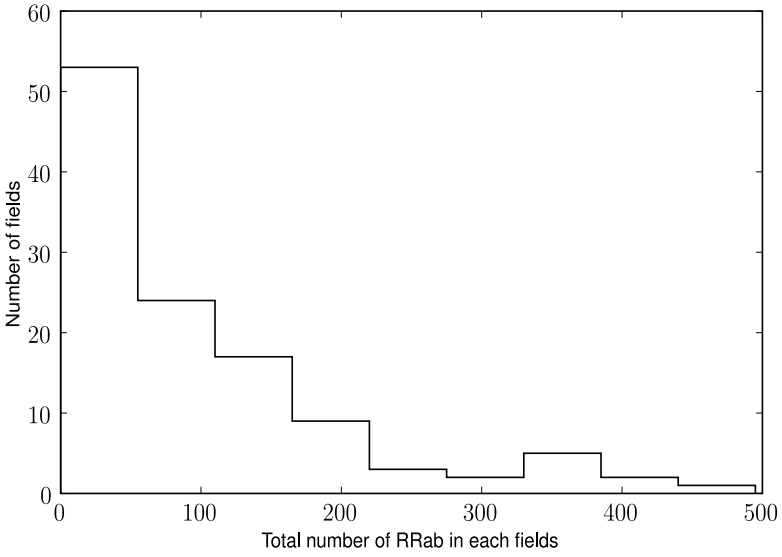

Figure 4.2: The histogram showing distribution of total number of long and short period RRab in our sample.

Criteria	Fields	Designated Number
$N_T < 204$	outer	3
$204 \leq N_T \geq 347$	intermediate	2
$N_T > 347$	inner	1

Table 4.1: The criteria used in categorising stars in the three groupings.

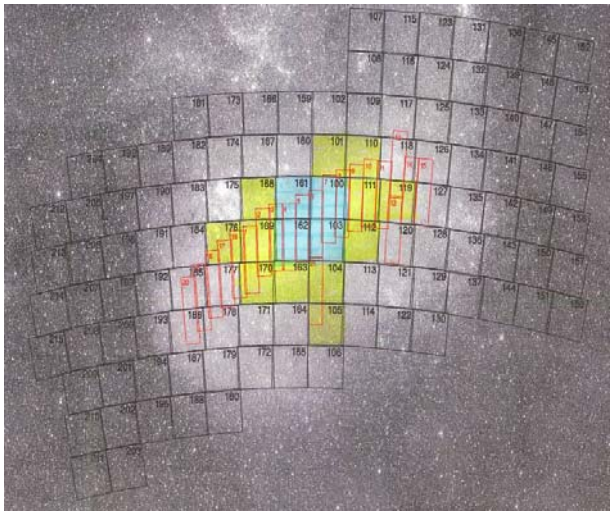

Figure 4.3: The area occuppied by RRab stars in our three groupings: Blue is for dense field(Inner); Yellow - Middle (Intermediate fields) and Unshaded areas are for Outer field stars.

Criteria	Fields	Designated Number
$N_T < 109$	outer	5
$109 \leq N_T < 204$		4
$204 \leq N_T < 268$		3
$268 \leq N_T < 368$		2
$368 \leq N_T < 500$	inner	1

Table 4.2: The criteria used in categorising stars in the five groupings.

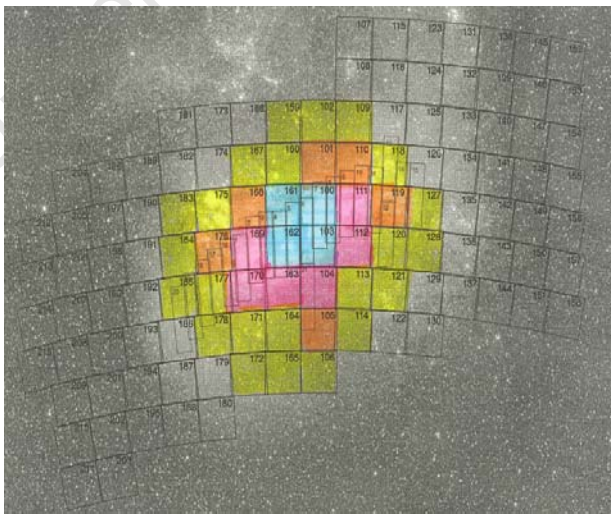

Figure 4.4: The area occuppied by RRab stars in our five groupings: Blue is for dense field(Inner); Yellow, red and orange - Middle (Intermediate fields) and Unshaded areas are for Outer field stars.

4.2 Part A-samples when the bright stars removed (16864)

Case	Period(days)	Period type	Number of stars
	P $<$ 0.544	short	5693
I	0.544 $\leq$ P $\geq$ 0.600	intermediate	5376
	P $>$ 0.600	long	5795
	P $<$ 0.514	short	3368
II	0.514 $\leq$ P $\geq$ 0.630	intermediate	10075
	P $>$ 0.630	long	3421
	P $<$ 0.485	short	1602
III	0.485 $\leq$ P $\geq$ 0.660	intermediate	13626
	P $>$ 0.660	long	1636

Table 4.3: The groupings in the three different cases for part A.

4.3 Three groupings-part A

We also calculated the galactocentric distance (R_{GC}), for the three groupings for part A (as described in chapter 3). We made plots of ratio of long to short period RRab stars vs R_{GC} in the same way as described before and the results were tabulated in Table 4.6, 4.7, 4.8 and later plotted in Figure 4.8, 4.9, 4.10.

Case	Period(days)	Fields	N(long)	N(short)	Ratio long to short
	P $<$ 0.544	Inner	789	841	0.94±0.05
I		Middle	1566	1648	0.95±0.03
	P $>$ 0.600	Outer	3440	3204	1.07±0.03
	P $<$ 0.514	Inner	467	510	0.92±0.06
II		Middle	905	1012	0.89±0.04
	P $>$ 0.630	Outer	2049	1846	1.11±0.04
	P $<$ 0.485	Inner	233	260	0.90±0.08
III		Middle	438	492	0.89±0.06
	P $>$ 0.660	Outer	965	850	1.14±0.05

Table 4.4: The ratio of long to short RRab in three different cases and three groupings for part A.

Case	Period	Fields	Fields	χ^2
	P < 0.544	Inner	Outer	7.2
I		Outer	Middle	9.3
	P >0.600	Inner	Middle	0.06
	P < 0.514	Inner	Outer	7.6
II		Outer	Middle	13.3
	P > 0.630	Inner	Middle	0.07
	P < 0.485	Inner	Outer	9.4
III		Outer	Middle	10.4
	P > 0.660	Inner	Middle	0.00001

Table 4.5: The χ^2 values for the different cases and fields for three groupings for part A, i.e. when the bright stars removed.

Regions	Mean R_{GC} (kpc)	Ratio of long to short	Error in the ratio
1	0.73	0.94	0.05
2	1.10	0.95	0.03
3	2.46	1.07	0.05

Table 4.6: The values of the calculated mean R_{GC} in the three groupings for part A in case I.

Regions	Mean R_{GC} (kpc)	Ratio of long to short	Error in the ratio
1	0.73	0.92	0.06
2	1.16	0.89	0.04
3	2.42	1.11	0.04

Table 4.7: The values of the calculated mean R_{GC} in the three groupings for part A in case II.

Regions	Mean R_{GC} (kpc)	Ratio of long to short	Error in the ratio
1	0.73	0.90	0.08
2	1.17	0.89	0.06
3	2.41	1.14	0.05

Table 4.8: The values of the calculated mean R_{GC} in the three groupings for part A in case III.

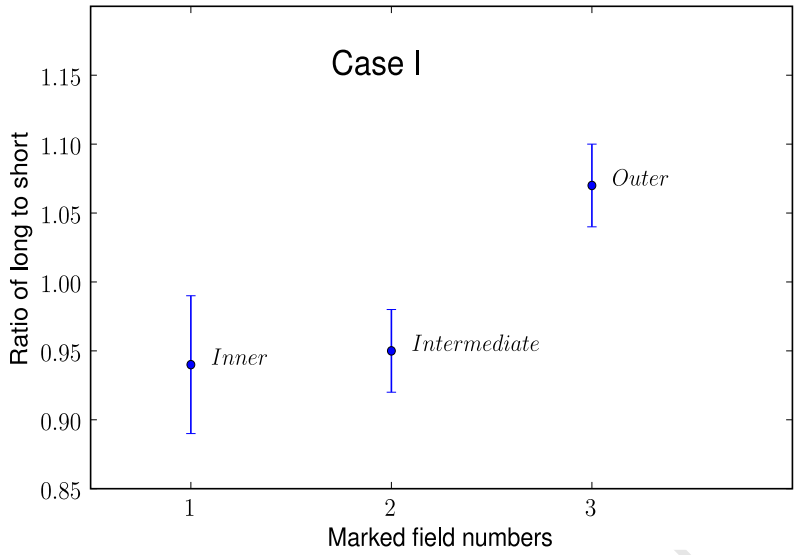

Figure 4.5: The ratio of long to short RRab stars for part A for three groupings.

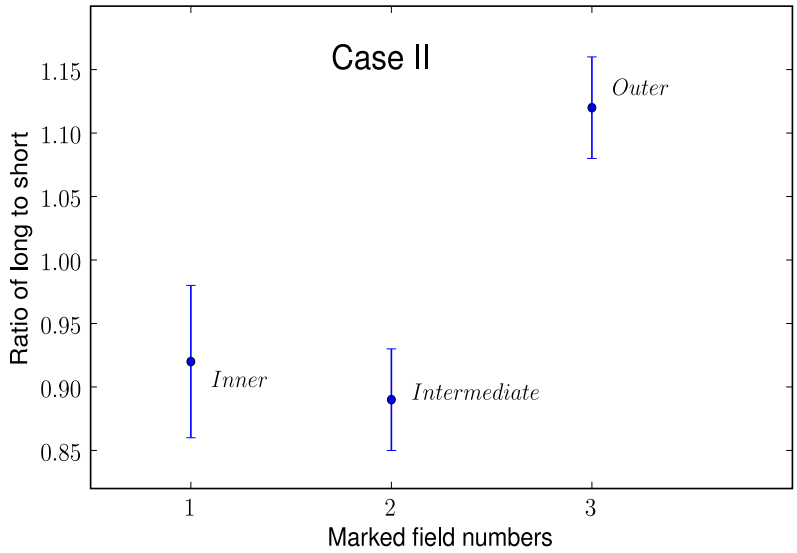

Figure 4.6: The ratio of long to short RRab stars for part A for three groupings.

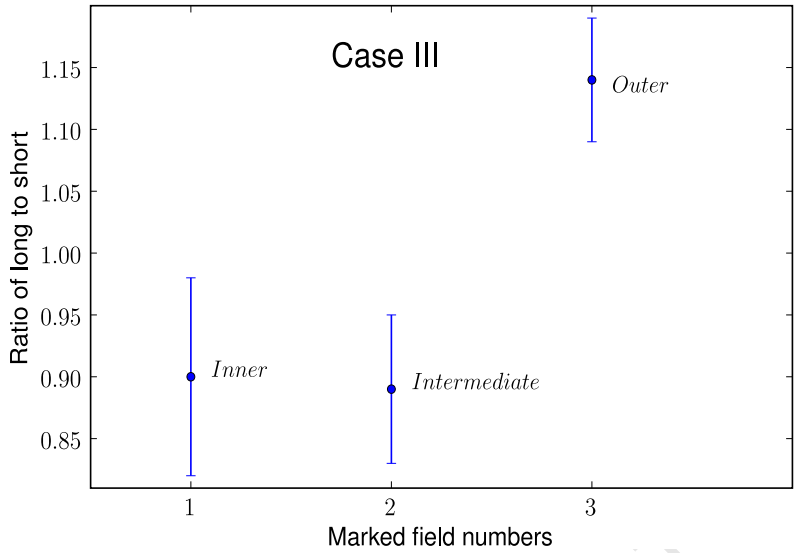

Figure 4.7: The ratio of long to short RRab stars for part A for three groupings.

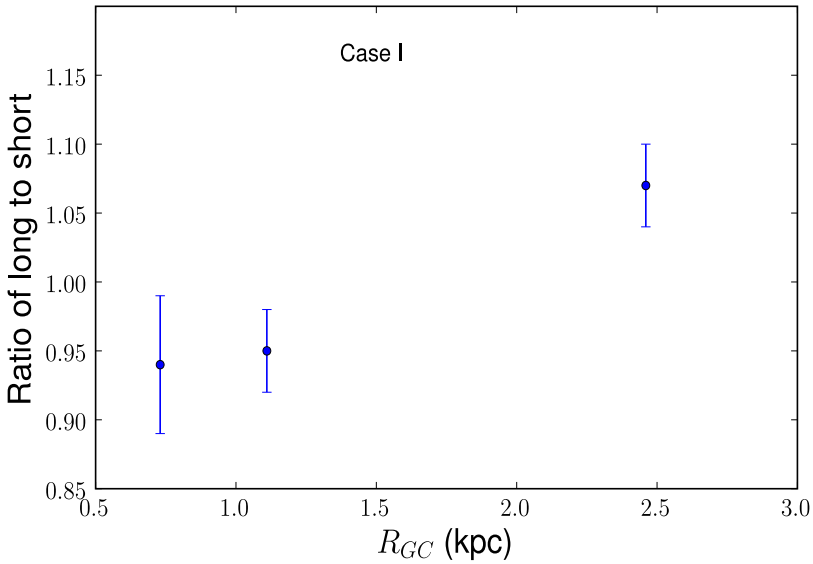

Figure 4.8: The ratio of long to short RRab stars against galactocentric distance calculated for the 3 groupings for part A - similar to Figure 4.5.

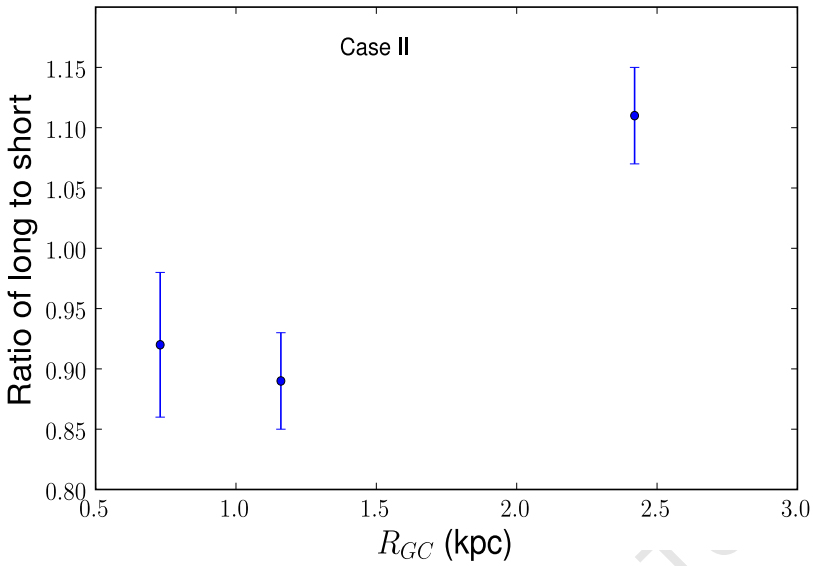

Figure 4.9: The ratio of long to short RRab stars against galactocentric distance calculated for the 3 groupings for part A - similar to Figure 4.6.

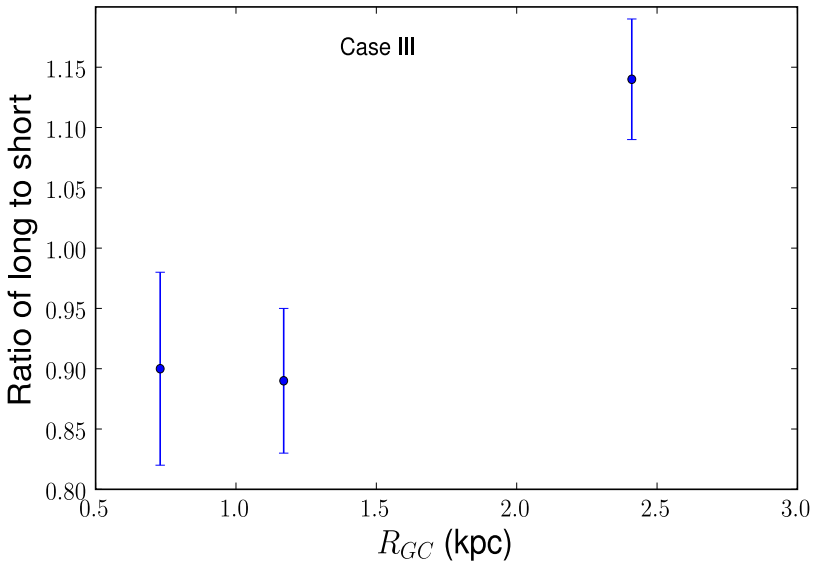

Figure 4.10: The ratio of long to short RRab stars against galactocentric distance calculated for the 3 groupings for part A - similar to Figure 4.7.

4.4 Conclusion on three groupings-part A

From the results we obtained from part A, three groupings for the three different cases, we found out that the ratio of long to short period RRab stars in the LMC increases outwards, i.e. from the centre to the outer fields as seen in Table 4.4, 4.6, 4.7, 4.8 and Figure 4.5, 4.6, 4.7, 4.8, 4.9, 4.10. When we tested for the significance differences in the period distribution among the RRab stars in the three different groupings, we found out that there was significance differences in the period distribution between the inner RRab stars and the outer RRab stars (χ^2 values of 7.2, 7.6 and 9.4 for case I, II and III respectively), but no significance differences in the period distribution between the inner and intermediate RRab stars (χ^2 values of 0.06, 0.07 and 0.1 for cases I, II and III respectively), and also significance differences in period distribution between the intermediate and outer RRab stars (χ^2 of 9.3, 13.3 and 10.4 for cases I, II and III respectively).

4.5 Five groupings-part A

The ratio of the number of long to short period RRab stars for the five groupings in the three different cases I, II, III as shown in Table 4.9 and the plots are in Figure 4.11 with the χ^2 test results in Table 4.10.

Case	Period(days)	Fields	N(long)	N(short)	Ratio of long to short
		1	789	841	0.94±0.05
	P < 0.544	2	920	948	0.97±0.05
I	P > 0.600	3	646	700	0.93±0.05
		4	1689	1653	1.02±0.04
		5	1751	1551	1.13±0.04
		1	467	510	0.92±0.06
	P < 0.514	2	534	573	0.93±0.06
II	P > 0.630	3	371	439	0.85±0.06
		4	1005	1005	1.00±0.05
		5	1044	841	1.24±0.06
		1	233	260	0.90±0.08
	P <0.485	2	251	280	0.90±0.08
III	P >0.660	3	187	212	0.88±0.09
		4	481	461	1.04±0.07
		5	484	389	1.24±0.08

Table 4.9: The ratio of long to short RRab in three different cases and five groupings for part A.

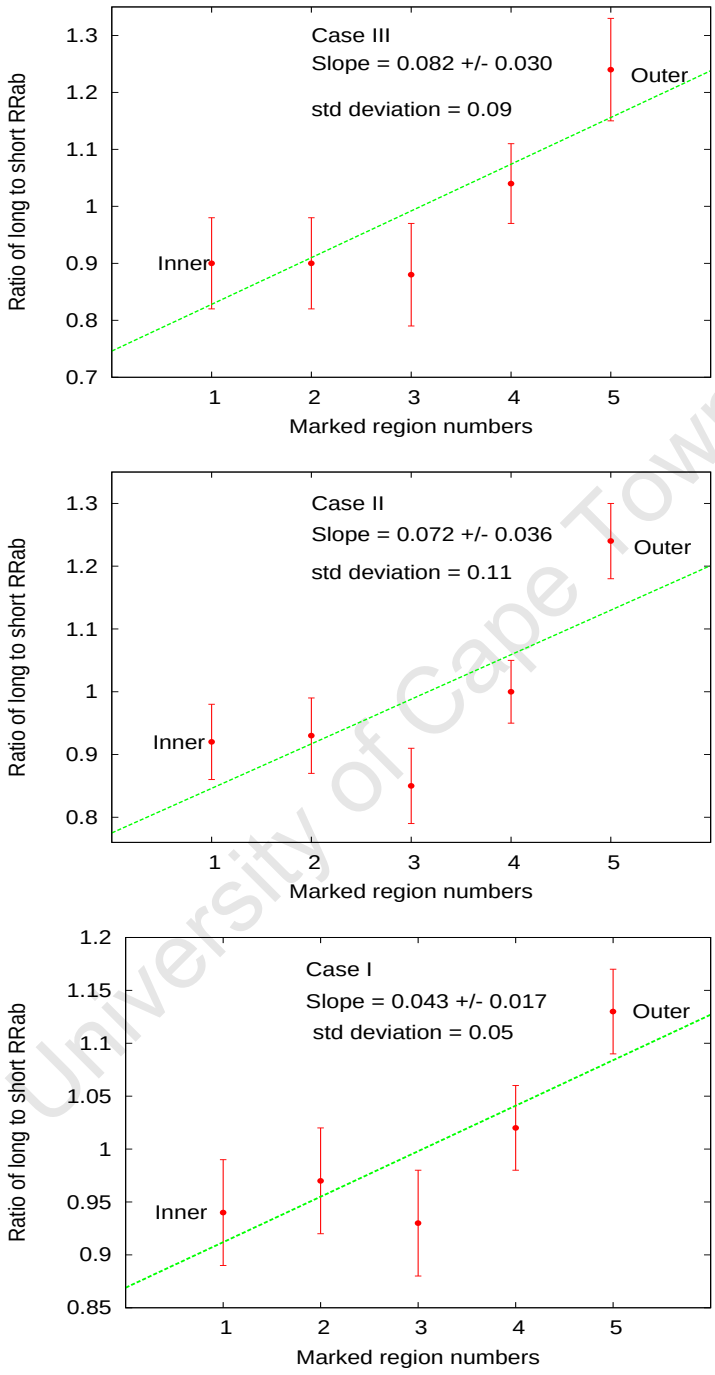

Figure 4.11: The ratio of long to short period RRab stars for five groupings for part A.

Fields	Fields	χ^2
1	2	0.3
	3	0.04
	4	1.5
	5	11.0
2	3	0.45
	4	0.79
	5	9.2
3	4	2.7
	5	10.0
4	5	4.9
5	1+2+3+4	13.7
Left	Right	0.12
Top	Bottom	0.014

Table 4.10: Testing for the significance difference between the different fields for five groupings and for the case where we have P $<$ 0.544 and P $>$ 0.600 for part A - 2 degrees of freedom.

4.6 Conclusion on five groupings-part A

From the results we obtained from part A, five groupings for the three different cases, we found out that the ratio of long to short period RRab stars in the LMC increases outwards, i.e. from the centre to the outer fields as seen in Table 4.9 and Figure 4.11. When we tested for the significance differences in the period distribution among the RRab stars in the different groupings for case I, we found out that there was significance differences in the period distribution between the inner RRab stars and the outer RRab stars (χ^2 values of 11.0 and 9.2 as seen in Table 4.10). χ^2 value of 0.12 was obtained when we tested for the significance differences in the period distribution among the RRab stars on the left and right side of the LMC. χ^2 value of 0.014 was obtained for the period distribution among the RRab stars on the top and bottom side of the LMC. From the two χ^2 values, we were not able to deduce whether there was significance differences in the period distribution or not. There is a suggestion of a flat distribution in the three inner bins but given the error bars, this does not seem significant.

4.7 Part B-samples containing the bright stars (17692)

In this second part of our analysis, we worked with samples containing the bright stars and carried out the analysis in the same way as described previously. The aim here was to see if including the bright stars had a significant effect on the results in part **A**.

Case	Period(days)	Period type	Number of stars
	P $<$ 0.544	short	5846
I	0.544 $\leq$ P $\geq$ 0.600	intermediate	5505
	P $>$ 0.600	long	5945
	P $<$ 0.514	short	3466
II	0.514 $\leq$ P $\geq$ 0.630	intermediate	10306
	P $>$ 0.630	long	3524
	P $<$ 0.485	short	1648
III	0.485 $\leq$ P $\geq$ 0.660	intermediate	13939
	P $>$ 0.660	long	1709

Table 4.11: The groupings in the three different cases for part B.

4.8 Three groupings-part B

Case	Period(days)	Fields	N(long)	N(short)	Ratio long to short
	P $<$ 0.544	Inner	829	888	0.93±0.05
I		Middle	1630	1694	0.96±0.03
	P $>$ 0.600	Outer	3486	3264	1.07±0.03
	P $<$ 0.514	Inner	494	534	0.93±0.06
II		Middle	882	984	0.90±0.04
	P $>$ 0.630	Outer	2148	1948	1.10±0.04
	P $<$ 0.485	Inner	252	269	0.94±0.08
III		Middle	427	471	0.91±0.06
	P $>$ 0.660	Outer	1030	908	1.13±0.05

Table 4.12: The ratio of long to short period RRab in three different cases and three groupings for part B.

This was followed by making plots showing how the ratio varies from the inner (dense field) to the outer fields for the three different cases as seen in Figures 4.12, 4.13, 4.14.

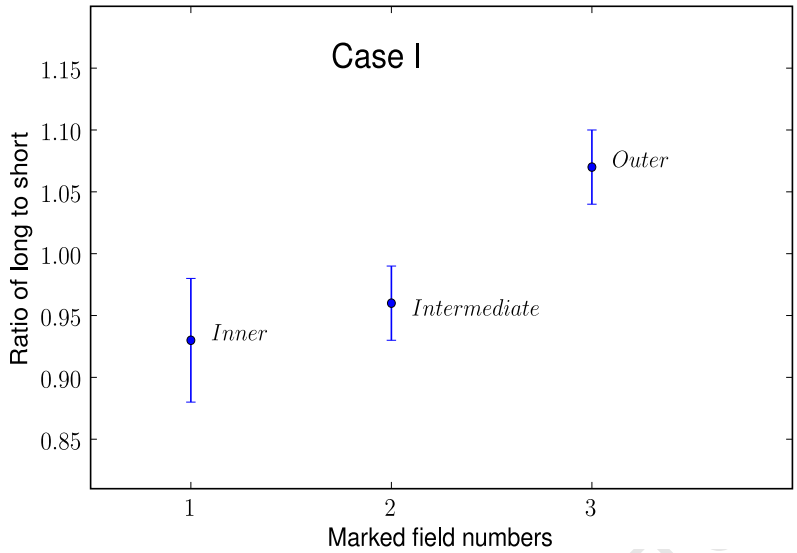

Figure 4.12: The ratio of long to short period RRab stars for three groupings for part B for case I.

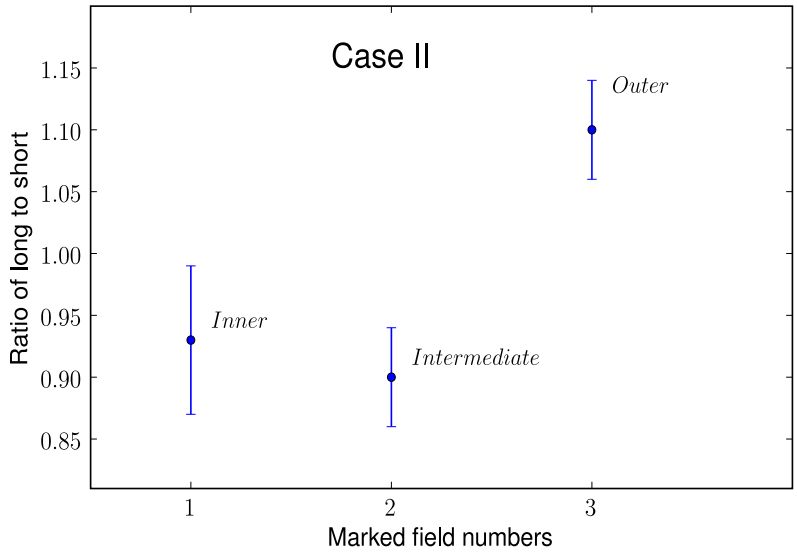

Figure 4.13: The ratio of long to short period RRab stars for three groupings for part B for case II.

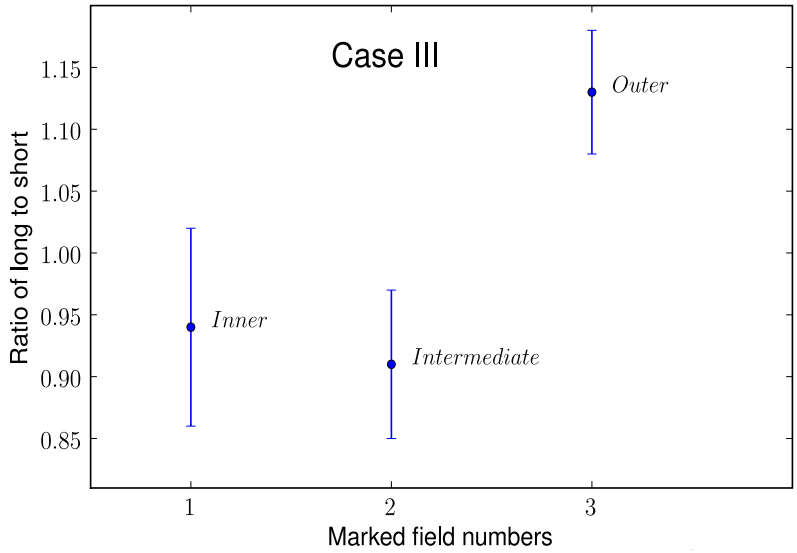

Figure 4.14: The ratio of long to short period RRab stars for three groupings for part B for case III.

Case	Period	Fields	Fields	χ^2
	P $<$ 0.544	Inner	Outer	6.6
I		Outer	Middle	6.4
		Inner	Middle	0.3
	P $>$ 0.600	Inner + Middle	Outer	9.6
		Outer + Middle	Inner	3.9
	P $<$ 0.514	Inner	Outer	6.7
II		Outer	Middle	14.1
	P $>$ 0.630	Inner	Middle	0.12
	P $<$ 0.485	Inner	Outer	4.1
III		Outer	Middle	7.9
	P $>$ 0.66	Inner	Middle	0.05

Table 4.13: The χ^2 values for the different cases and fields for three groupings for part B - 2 degrees of freedom.

4.9 Conclusion on three groupings-part B

From the results we obtained from part B, three groupings for the three different cases, we also found out that the ratio of long to short period RRab stars in the LMC increases outwards, i.e. from the centre to the outer fields as seen in Table 4.12 and Figure 4.12, 4.13, 4.14 . When we tested for the significance differences in the period distribution among the RRab stars in the three different groupings, we found out that there was significance differences in the period distribution between the inner RRab stars and the outer RRab stars (χ^2 values of 6.6, 6.7 and 4.1 for case I, II and III respectively), but no significance differences in the period distribution between the inner and intermediate RRab stars (χ^2 values of 0.3, 0.12 and 0.05 for cases I, II and III respectively), and also significance differences in period distribution between the intermediate and outer RRab stars (χ^2 of 6.4, 14.1 and 7.9 for cases I, II and III respectively).

4.10 Five groupings-part B

Case	Period(days)	Fields	N(long)	N(short)	Ratio of long to short
		1	829	888	0.93±0.05
	P < 0.544	2	952	984	0.97±0.04
I	P > 0.600	3	678	710	0.96±0.05
		4	1712	1700	1.01±0.03
		5	1774	1564	1.13±0.04
		1	494	534	0.93±0.06
	P < 0.514	2	552	598	0.92±0.06
II	P > 0.630	3	393	441	0.89±0.06
		4	1029	1035	0.99±0.05
		5	1056	858	1.23±0.06
		1	252	269	0.94±0.08
	P < 0.485	2	263	294	0.89±0.08
III	P > 0.660	3	201	205	0.98±0.09
		4	493	483	1.02±0.07
		5	500	397	1.26±0.09

Table 4.14: The ratio of long to short RRab in three different cases and five groupings for part B.

Fields	Fields	χ^2
	2	0.32
1	3	0.12
	4	1.6
	5	10.8
	3	0.02
2	4	0.56
	5	7.9
	4	0.02
3	5	0.86
4	5	6.0
5	1+2+3+4	14.6
Left	Right	2.6
Top	Bottom	0.008

Table 4.15: Testing for the significance difference between difference fields for five groupings and for the case where we have P < 0.544 and P > 0.600 for part B - 2 degrees of freedom.

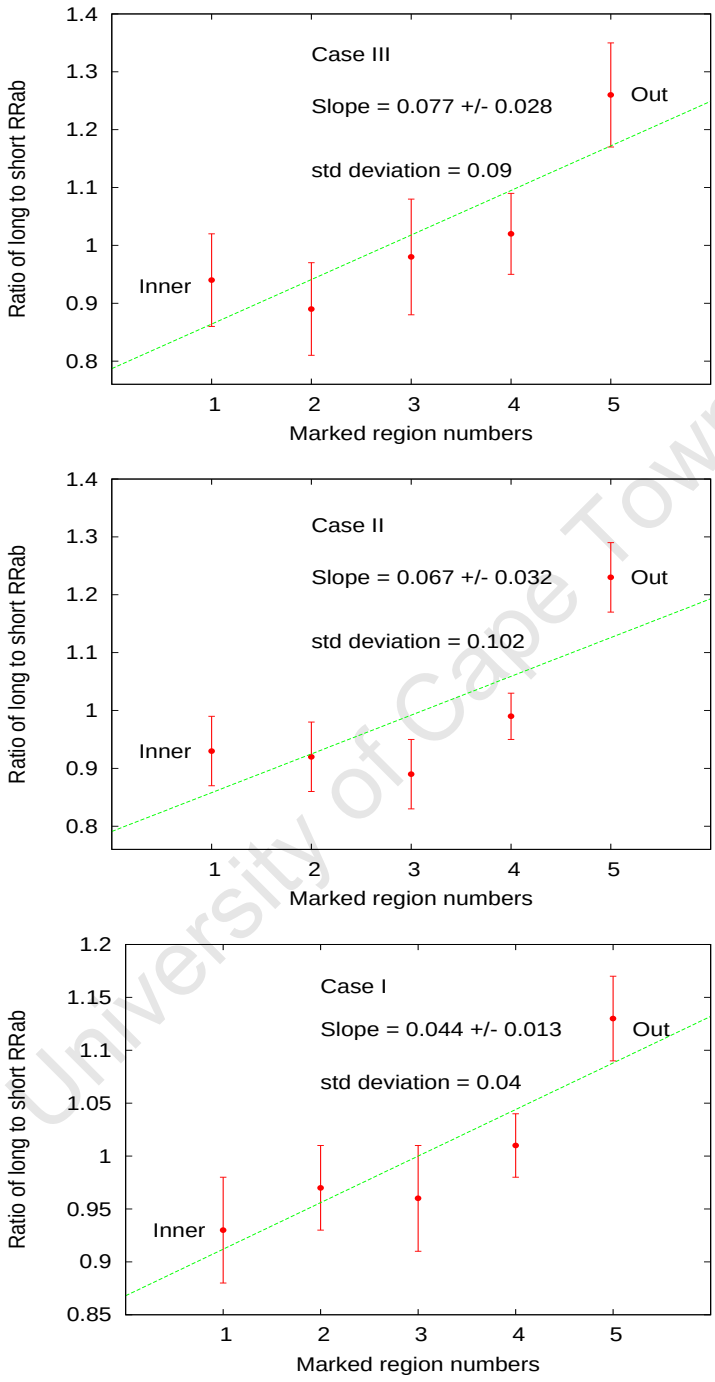

Figure 4.15: The ratio of long to short period RRab stars for five groupings for part B.

4.11 Conclusion on five groupings-part B

From the results we obtained from part B, five groupings for the three different cases, we found out that the ratio of long to short period RRab stars in the LMC increases outwards, i.e. from the centre to the outer fields as seen in Table 4.14 and Figure 4.15. When we tested for the significance differences in the period distribution among the RRab stars in the different groupings for case I, we found out that there was significance differences in the period distribution between the inner RRab stars and the outer RRab stars (χ^2 values of 10.8 and 7.9 as seen in Table 4.15). χ^2 value of 2.6 was obtained when we tested for the significance differences in the period distribution among the RRab stars on the left and right side of the LMC. χ^2 value of 0.008 was obtained for the period distribution among the RRab stars on the top and bottom side of the LMC. From the two χ^2 values, we were not able to deduce whether there was significance differences in the period distribution or not.

4.12 Main conclusion

Omitting or including bright stars does not change our conclusion.

4.13 General conclusion on the selection according to space density

Since Figure 2.1 shows metallicity decreases with increasing period, an increase in the long/short ratio implies a decrease in the metallicity of the sample. In both part A and B, our results are interpreted in the following ways ;

1. We interprete the ratio of long to short RRab stars increasing from the LMC centre in terms of metallicity gradient; whereby the metallicity gradient increases inwards. In other words, the LMC centre is more metal rich than the outer part.

2. From the χ^2, we conclude that there is a significance differences in the period distribution between the outer and inner field RRab stars, intermediate and outer field RRab stars while no significance difference in the period distribution between inner and intermediate field RRab stars was detected by this method.

The results from **part A** and **B** indicate that there is a metallicity gradient in the LMC Lyrae population with the variables in the outer parts of the Cloud having lower metallicities than those nearer the centre. We therefore conclude that there is a reasonable evidence for a mild decrease in mean metallicity of the LMC RRab population with increasing distance from the centre.

Thus qualitatively at least the RRab stars in the outer parts of the LMC are on average more metal poor than those in the inner region.

Chapter 5

Conclusions and recommendations

5.1 General conclusion

In this project we studied the metallicity distribution in the Large Magellanic Cloud (LMC) using the RR Lyrae (RRab) data from the Optical Gravitational Lensing Experiment with a [Fe/H]-period relation.

We found out that the metallicity of this old population decreases with increasing distance from the centre of the Large Magellanic Cloud with the metallicity gradient defined of either -0.015±0.003× R_{GC} or -0.010±0.002× R_{GC} depending on the calibration of [Fe/H]-period relation of the LMC RRab stars.

We also found out that by introducing phase or amplitude did not improve on the [Fe/H]-period formula.

We carried out further test by deriving the ratio of the number of long to short period RRab stars as a function of density of the individual fields. This showed a significance differences in the period distribution between the inner and outer field RRab stars.

We also found out that omitting or including bright stars does not change our conclusion.

5.2 Future work and recommendation

In this project we carried out study on the metallicity distribution in the LMC using the fact that the metallicity of RRab stars depends entirely on period. There is a need to confirm this result using observational data by measuring the metallicity of RRab stars in the OGLE III data base by spectroscopy.

This therefore, calls for the use of Large Telescopes like the Southern African Large Telescope (SALT) to do this kind of science since it has got a Prime Focus Imaging Spectrograph which will be able to measure the metallicities and radial velocities of RR Lyrae stars (RRab) from their spectra. We think that this will advance our understanding of the structure and evolution of the LMC.

Appendix

χ^2 test and statistical analysis

This test compares any three or more groups or classes of things. It compares matched observation made on a single random sample group, for evidence of association between two qualities, when at least one of these qualities is divided into three or more categories, e.g. short, intermediate and long (Russell, 1970).

As reported by Moroney (1956), χ^2 test can be calculated or estimated as shown below. The information is as summarised in Table 5.1.

Then,

	A	B	Totals
Group 1	a	c	e
Group 2	b	d	f
Totals	g	h	k

Table 5.1: A typical way of calculating χ^2 values, adopted from Russell (1970), page 255

$$\chi^2 = \frac{(bc - ad)^2 k}{efgh}. \tag{5.1}$$

Where a and b are the number of items in observation A in group 1 and 2, while c and d are the respective number of items in observation B in group 1 and 2.

However, in 1934, Yate tested the accuracy of the above formula by applying a correction to Table 5.1. The reason behind this is because χ^2 is a continous distribution and by applying the correction, we are actually decreasing by $\frac{1}{2}$ those values in our table which exceed expectation and increasing by $\frac{1}{2}$ those values which are less than the expected value (Moroney, 1956). The above table and formula become;

	A	B	Totals
Group 1	a - 0.5	c + 0.5	e
Group 2	b + 0.5	d - 0.5	f
Totals	g	h	k

Table 5.2: Testing the accuracy of χ^2 after applying Yate's correction, adopted from Russell (1970), page 255

$$\chi^2 = \frac{[(b+0.5)(c+0.5) - (a-0.5)(d-0.5)]^2 k}{efgh}. \tag{5.2}$$

Interpretation of χ^2 values

The graph of χ^2 tells us how good or bad the fit is between two qualities. The 0.1%, 1% and 5% levels indicate suspiciously **bad** fit while 95% and 99% are used to indicate suspiciously **good** fit, i.e. Moroney (1956), page 253.

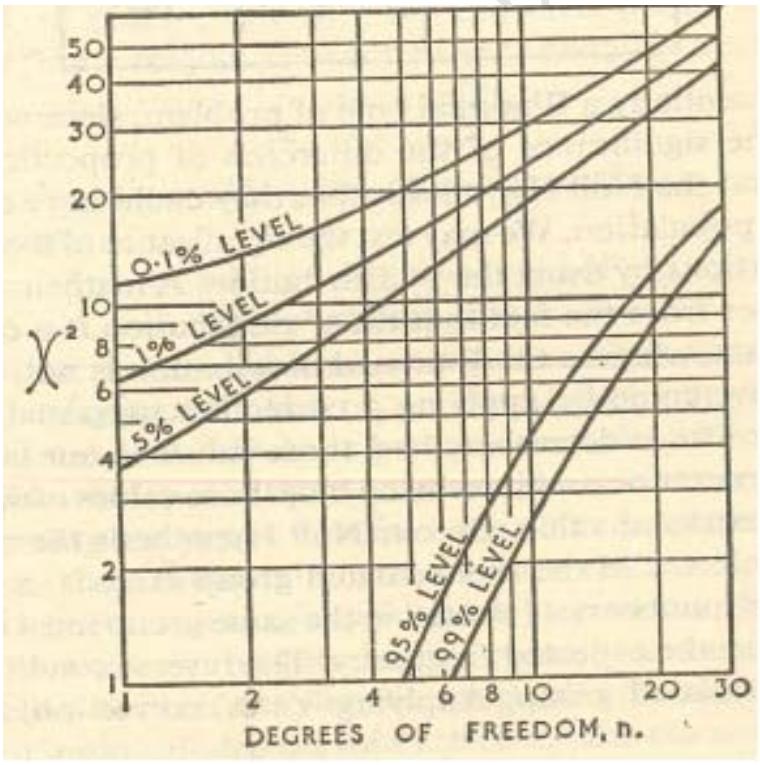

Figure 5.1: Interpretion of χ^2. Adopted from Moroney (1956)

Maximum Likelihood (ML) Method

The Maximum Likelihood (ML) method is a technique that is used for searching for the coefficients of relations of the form;

$$y = \alpha x + \beta z + \gamma. \tag{5.3}$$

Where α, β and γ are the coefficients to be determined, y is the dependent variable , x and z are the independent variables. The method works in a situation where the values of dependent and independent variables are known and the standard error of one observation of each quantities x and z (independent variables) are also known.

Bibliography

Alcaino, G. 1975, A&AS, **21**, 279

Alcock, C. et al., 2000, AJ, **119**, 2194

Allen, D. A. 1980, Astrophysical Letters, **20**, 131

Battinelli, P., & Demers, S. 2005, A&A, **434**, 657

Benny, J., & Merrifield, M. 1998, Galactic Astronomy, Princeton, New Jersey, USA

Bevington, P. R. 1969, McGraw-Hill Book company, New York, USA

Borissova, J. et al., 2006, A&A, **460**, 459

Buscombe, W. 1954, ASPL, **7**, 3

Byrd, G. et al., AJ, **107**, 2055

Carrera, R. et al., 2008, AJ, **135**, 836

Carroll, B. W., & Ostlie, D. A. 1996, An introduction to Modern Astrophysics, Addison - Wesley

Clementini, G. et al., 2003, AJ, **125**, 1309

Cioni, M. -R. L. 2009, A&A, **506**, 1137

Cioni, M. -R. L., & Habing, H. J. 2003, A&A, **402**, 133

Di Fabrizio, L. et al., 2005, A&A, **430**, 603

Eddington, A. S. 1926, The internal constitution of stars, Cambridge University Press

Feast, M. W. 1968, MNRAS, **140**, 345

Feast, M. W. et al., 1960, MNRAS, **121**, 337

Gautschy, A., & Saio, H. 1995, Anul.Rev.Astron.Astrophys, **33**, 75

Gratton, R. G. et al., 2004, A&A, **421**, 937

Grocholski, A. J. et al., 2006, AJ, **132**, 1630

http://ogle.astrouw.edu.pl/main/tel.html

Iben, I. 1974. Stellar Instability and Evolution, IAU symposium **59**, 3

Jurcsik, J., & Kovács, G. 1996, A&A, **312**, 111

Kholopov, P. N. et al., 1985, General Catalogue of Variable Stars, Fourth Edition, (Moscow)

King, D. S., & Cox, J. P. 1968, PASP , **80**, 365

Layden, A. C. 1995, AJ, **110**, 3212

Lee, K. M., & Schmidt, E. G. 2001, PASP, **113**, 1140

McCarthy, F. D. 1956, Australia's Aborigines Their Life and Culture (Colourgravure Publications, Melbourne, Australia)

Murai, T., & Fujimoto, M. 1980, PASJ, **32**, 581

Moroney, J. 1956, Facts from Figures, Penguin books, third edition

Nikolaev, S. 2006, MNRAS, **366**, 1503

Pagel, B. E. et al., 1978, MNRAS, **184**, 569

Pigafetta, A. 1524, Magellan's Voyage A Narrative Account of the first Navigation (translated by R.A. Skelton, The Folio Society, London, 1975)

Poleski, R. et al., 2010, Act.Ast, **60**, 1

Ritter, A. 1879, Ann. Phys. Chem. Neue Folge, 8, 157

Russell, L. 1970, Practical Statistics, Pan books Ltd - London, second edition

Sandage, A. 1993, AJ, **106**, 687

Sandage, A. 1961, The Hubble atlas of galaxies, Washington: Carnigie Institution

Sarajedini, A. et al., 2006, AJ, **132**, 1361

Simon, N. R., & Lee, A. S. 1981, AJ, **248**, 291

Smart, W. M. 1977, Text-Book on spherical astronomy, Cambridge University Press, 6th edition

Smith, H. A. 1995, RR Lyrae stars, Cambridge University Press, first edition

Soszyński, I. et al., 2009, Act.Ast, **59**, 1

Soszyński, I. et al., 2008a, Act.Ast, **58**, 163

Soszyński, I. et al., 2008b, Act.Ast, **58**, 293

Soszyński, I. et al., 2003, Act.Ast, **53**, 93

Thackeray, A. D., & Wesselink, A. J. 1953, Nature, **171**, 693

Udalsi, A. 2003, Act.Ast, **53**, 291

Van Der Marel, R. P., & Cioni, M-R. L. 2001, AJ, **122**, 1807

Van Der Marel, R. P. et al., 2002, AJ, **124**, 2639

Van Leeuwen, F. et al., 2007, MNRAS, **379**, 724

Westerlund, B. 1997, The Magellanic Cloud, Addison - Wesley